Design of a Suction-Based Wall-Climbing Robot for Installing NDT Sensors on Dry Cask Storage Tanks

by

Ethan Elgavish

THESIS

Presented to the Faculty of the Graduate School of

The University of Texas at Austin

in Partial Fulfillment

of the Requirements

for the Degree of

MASTER OF SCIENCE IN ENGINEERING

THE UNIVERSITY OF TEXAS AT AUSTIN

December 2023

The Thesis Committee for Ethan Elgavish
Certifies that this is the approved version of the following thesis:

Design of a Suction-Based Wall-Climbing Robot for Installing NDT Sensors on Dry Cask Storage Tanks

APPROVED BY

SUPERVISING COMMITTEE:

Mitch Pryor, Co-Supervisor

Salvatore Salamone, Co-Supervisor

Acknowledgments

First and foremost, my deepest appreciation goes to my mentors, Dr. Pryor, Dr. Anderson, and Dr. Salamone. Their collective expertise, unwavering support, and invaluable guidance have been foundational to my academic and personal growth. Their dedication to my progress and consistent feedback have been pivotal in the realization of this thesis.

I am indebted to my collaborators, Nathan Wilson, Zack Jurecek, Ryan Lee, and Tony Lee, for their invaluable contributions and insights. Additionally, I extend my gratitude to all the students in the Nuclear and Applied Robotics Lab; your collective wisdom, camaraderie, and support have made this journey enriching and memorable.

Special acknowledgment is due to all the undergraduate students who participated in the earliest stages of this project through the senior design program. Your dedication, fresh perspectives, and hard work laid the groundwork for what this research has become.

The financial backing of NEUP played a significant role in facilitating this research, and for that, I am profoundly grateful.

On a personal level, I wish to express my heartfelt appreciation to my partner, whose unwavering belief in me and patient understanding have been sources of strength and motivation. To my family, whose unconditional love and constant

encouragement have been my foundation throughout this endeavor: thank you for always being there.

Abstract

Design of a Suction-Based Wall-Climbing Robot for Installing NDT Sensors on Dry Cask Storage Tanks

Ethan Elgavish, M.S.E.
The University of Texas at Austin, 2023

Supervisors: Mitch Pryor
Salvatore Salamone

Spent Nuclear Fuel (SNF) is contained within welded Dry Storage Canister (DSC), comprised of a stainless-steel canister encased within a concrete overpack, to effectively contain radioactive materials. As the DSC's lifespan increases, the need for robust, comprehensive inspection and maintenance procedures becomes increasingly critical to detect and mitigate any potential degradation [1]. Traditional certification of DSCs currently relies on periodic visual inspections performed by experts, a method that has potential for enhancement through more frequent or continuous surveillance, paired with more objective and verifiable evaluation measures. Driven by these needs, the Smart Structures Lab, under the leadership of Dr. Salamone, has pioneered an innovative method for scrutinizing the condition of stainless-steel canisters. This approach employs an array of cost-effective piezoelectric sensors adhered to the canister's surface [2]. This thesis builds upon this work by developing and

evaluating a suction-based wall-climbing robot, integrated with a sensor deployment mechanism. The resulting system facilitates sensor installation, thereby enabling long-term, continuous monitoring of the DSC's condition. This effort focuses on two novel requirements for this task relative to other wall climbing robots: maintaining adhesion with low clearances (< 4") on non-ferromagnetic curved surfaces and robustly deploying sensors for long-term data collection.

Table of Contents

List of Tables

List of Figures

Acronyms

BLDC Brushless DC. xii, 44, 45

CFD Computational Fluid Dynamics. xii, 12, 25, 43–45

DOF Degrees of Freedom. 13

DSC Dry Storage Canister. vi–viii, xi, 1–5, 7–9, 13–16, 22, 26–29, 42, 49, 62, 68, 69

PWM Pulse Width Modulation. 59

PZT Piezoelectric. ix, 4, 15, 16, 28, 29, 68

RPM Revolutions Per Minute. 44

SciPy Scientific Python Package. 37

SNF Spent Nuclear Fuel. vi, 1, 2, 4

TPU Thermoplastic Polyurethane. xii, 12, 45, 47

Chapter 1

Introduction

As of February 2023, the U.S. Energy Information Agency reported that nuclear power generation constituted 18.2% of all electrical power production in the United States [3]. This power generation process yields waste in the form of Spent Nuclear Fuel (SNF), which, as of now, lacks a permanent disposal solution. A report by the US Government Accountability Office in September 2021 revealed the existence of 86,000 metric tons of SNF stored at 75 different sites throughout the country [4].

1.1 Nuclear Waste Storage

The current standard for SNF storage is the utilization of Dry Storage Canister (DSC). Each DSC is composed of a stainless-steel cylindrical canister, filled with an inert gas, and encased within a concrete overpack to safely contain the hazardous radioactive materials [1]. There is an open space between the canister and the overpack called the annulus, and this space is connected to the outside via air vents for cooling and ventilation. Over the course of a DSC's service life, susceptibility to corrosion and cracking is a major concern. The canisters are originally designed and certified for up to a 40-year lifespan, but with the absence of a permanent disposal solution,

the canisters need recertification or the SNF must be transferred to new canisters at the end of this lifespan [3]. The standard SNF disposal process is shown in Figure 1.1.

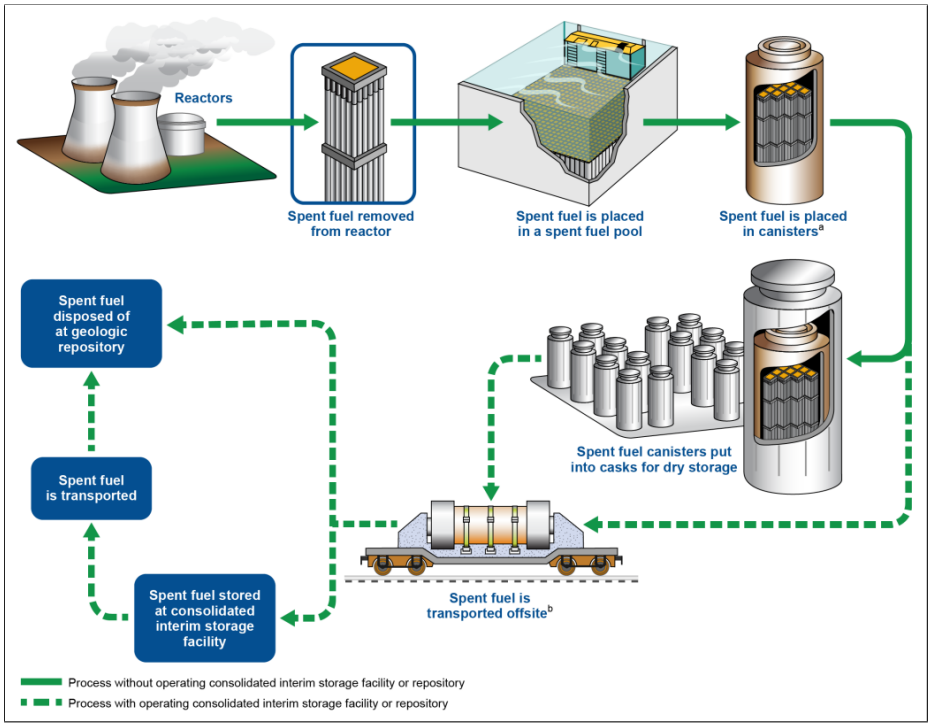

Figure 1.1: Storage of Nuclear Waste [4].

1.2 Prior Robotic Dry Cask Storage Inspection Solutions

As in-service DSCs age, the necessity for rigorous and comprehensive inspection and maintenance procedures increases, to detect and address any potential degradation. The standard certification procedure for DSCs relies on periodic expert visual inspections, often involving robotic systems equipped with a variety of sensors. There are many works that use robotic systems to assist in the inspection of the internal

condition of DSC canisters. However, most that were found in this literature search applied robot systems to vertical casks exclusively [5] [6] [7] [8] [9]. The approach is simpler for vertical applications than for horizontal applications, as the robotic system can remain suspended from a tether during the full range of operation (Figure 1.2). This thesis report focuses on the horizontal cask application, as there is less literature available in which it has been addressed. Applying a robotic system to a horizontal cask requires robust wall adhesion, as the system must be inverted to reach the full surface of the canister. This is further complicated by the small gap and non-ferromagnetic surface.

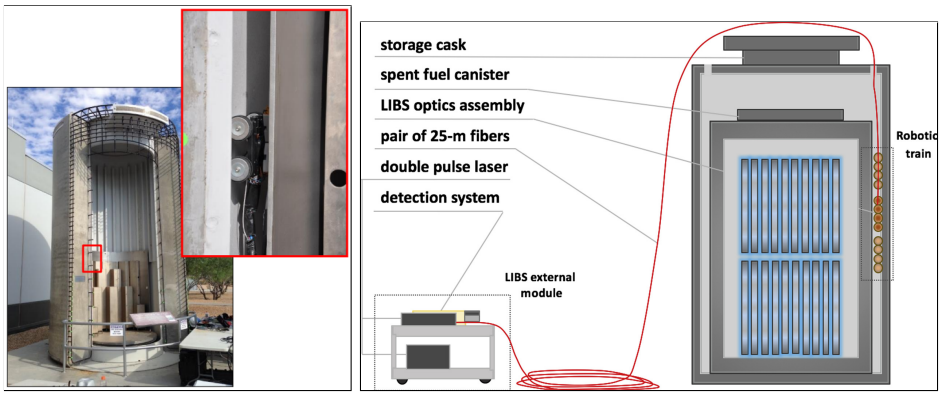

(a) EPRI Report [5] (b) Fobar et al. [6]

Figure 1.2: DSC inspection systems.

1.3 Summary of Overall Proposed Research Objectives

Along with the vertical cask constraint, the current robot aided inspection methodologies are often not ideal for two main reasons. The first is that they require a point to point inspection of the entire surface of the cask and therefore are time

consuming and inefficient. The second is that since degradation in dry cask system components accumulates over time, periodic inspections may not be the most effective way to pinpoint areas needing urgent preventative attention to combat component degradation and ensure safe long-term SNF storage.

Motivated by these requirements, the pioneering work conducted by Dr. Salamone and the Smart Structures Group has introduced an innovative approach to enable continuous and autonomous real-time monitoring of the condition of DSCs [2]. This methodology utilizes an array of cost-effective and low profile Piezoelectric (PZT) sensors affixed to the surface of the canister. Their solution enables integrated real-time sensing of the state of the cask using helical guided ultrasonic wave technology. By utilizing many echoes of a single ultrasonic wave (Figure 1.3), this methodology allows a small number of PZT sensors to generate information about the entire surface of the cylindrical cask. The added capabilities include the monitoring of internal pressure and temperature profiles, the detection of helium leakages, and the detection of stress corrosion cracking. The capability for continuous monitoring also allows for the detection of the onset conditions of leaks or cracking, preventing catastrophic failures and allowing for more cost effective applications of mitigation strategies.

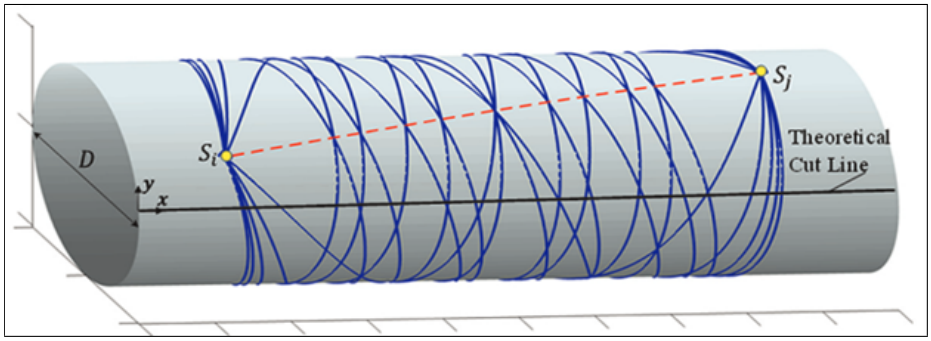

Figure 1.3: Helical wave approach for monitoring cylindrical structures [2].

This thesis report aims to aid in this groundbreaking research by concentrating on the remote deployment of the sensors on the surface of the cask. This goal requires two major capabilities to be developed, accessing the desired location on the cask and securely affixing a sensor to its surface. The resultant system facilitates the seamless installation of these sensors, allowing long-term and uninterrupted monitoring of the DSC's condition.

1.4 DSC Details and Description of Requirements

This section delves into the specific requirements essential for any system designed to navigate a DSC. The work in this study is aimed at the requirements imposed by the NUHOMs DSC system operated by Orano. Orano has provided a slice of a cask built to industry standard specifications as shown in Figure 1.4a, and these specifications are listed below. However, DSC systems exist in both vertical and horizontal orientations, as shown in Figure 1.4b. Therefore, the system described in this work is designed to be usable in both canister orientations.

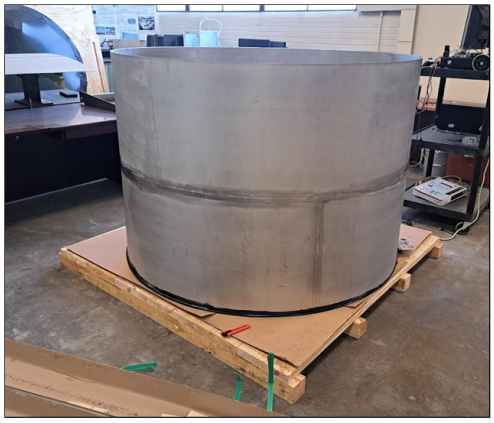

(a) Orano cask mock-up.

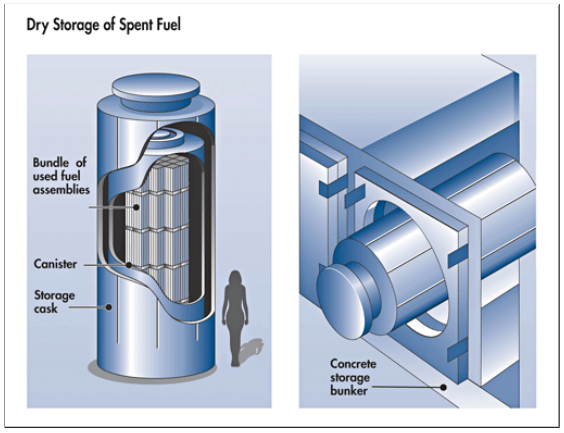

(b) Dry Storage Casks [1].

1.4.1 Geometric

The geometric constraints imposed by the system are listed as follows:

1. Curved Surface (67.25 inch diameter)
2. Non-Magnetic (stainless steel grades 304, 304L, and 316L)
3. Smooth surface condition
4. Height (4 inches)

The height constraint is determined for a specific NUHOMS cask design but is indicative of a general lack of vertical space for all cask orientations. The height constraint is defined by the height of the entrance point of the air vent to the annulus of the cask. This constraint varies widely for different cask installations, a height constraint of 4 inches encompasses most horizontal cask installations whereas a height constraint of 2 inches encompasses most vertical cask installations as well.

The stainless steel material and the 67.25 inch diameter are standardized and can be expected for both vertical and horizontal installations.

1.4.2 Temperature

The surface of the cask and the annulus between the cask and the overpack are very high in temperature as the nuclear fuel continues to generate heat long after it is removed from the power plant.

According to Wu et al. [10], the temperature of the surface of the canister drops from about 410 K (278 °F) to about 330 K (134 °F) over a 50-year period, with most of that decrease happening in the first 10 years. The temperature of the air in the annulus drops from about 310 K (98 °F) to about 300 K (80 °F) in the same period. This information informed the choice of materials for the surface-contacting components of the design and may result in a restriction to operating on older cask installations.

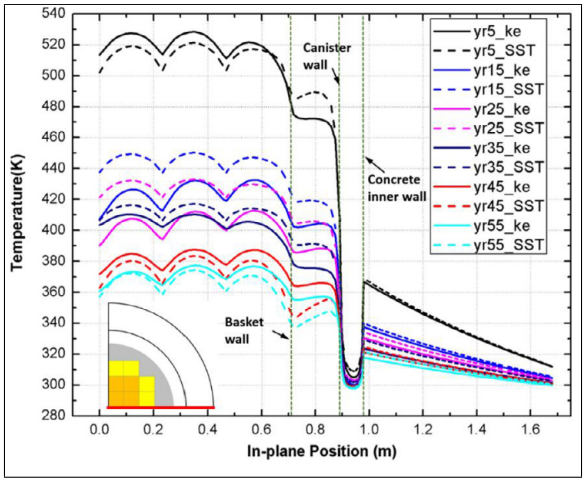

Figure 1.5: Dry Storage Canister Temperature [10].

1.4.3 Radiation Survivability

When navigating the cask's annulus, the system will encounter high gamma radiation levels. Alpha and beta particles are unlikely to penetrate the canister's half-inch thick stainless steel exterior. To determine the gamma radiation tolerance needed for the system, we refer to existing research. In 2007 P. L. Winston [11] measured the gamma radiation dose both in the annulus and at the surface of an active DSC. The cask inspected in this work had a 3.5 inch thick canister, so may underestimate the dose expected in a modern cask, but still provides a good baseline for understanding the radiation survivability requirements of the system. It was commissioned in 1989, and was 18 years old at the time of inspection. The study measured a maximum dose of approximately 2300 Roentgen per hour within the annulus. For perspective, the average annual dose per person from all man-made and natural sources is 620 millirem [12], which converts to 0.7 Roentgen per year. It also showed that the measured dose inside the annulus is very correlated with the dose measured on the surface of the concrete overpack, as demonstrated in Figure 1.6. This requirement is important to understand when designing a system that operates in a high radiation environment, but for this report, radiation survivability testing is not within the scope of this thesis.

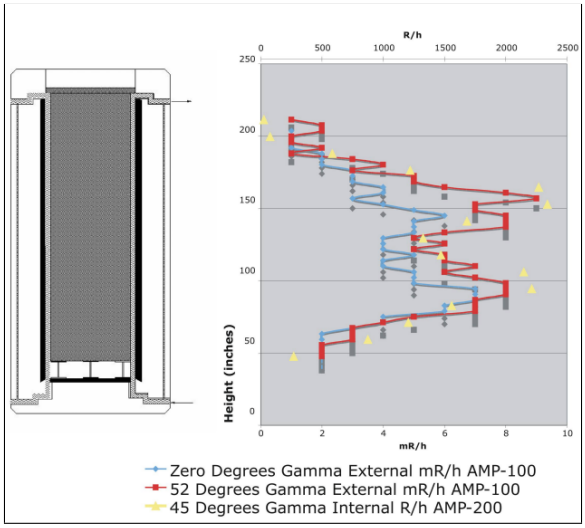

Figure 1.6: Dry Storage Canister Radiation Measurements [11].

1.4.4 Sensor Installation

The sensor deployment system must meet the following requirements. It must be able to carry multiple sensors at a time and attach them to the surface of the cask in series, this ensures that the application of many sensors remains efficient and could allow for multiple sensors to be installed with relative accuracy using robot localization algorithms. The system must be easily reloadable and deploy sensors with minimal user input and control, this allows the system to be used efficiently by a relatively inexperienced operator without failure.

1.4.5 Functional

There are several more functional requirements that are necessary for the successful application of the robot. During operation, the cables to the sensors must

not become tangled. This requirement can be addressed with a careful design of the sensor deployment mechanism and robot trajectory planning. The robot must work in all orientations about the horizontal canister. This includes the suction force necessary to adhere to the surface, install a sensor, and lift the cables attached to the sensors. The force required to install a sensor is dependent on the adhesive used to install it, which will be discussed in a later section. The signal processing that the Smart Structures Group does is highly dependent on signal quality, so for our purposes the sensor wires are a static requirement (20 AWG TE Piezoelectric Spiral Wrapped Coaxial Cable). The cables have a mass of 14.5 grams per meter, and the maximum height that they must be lifted in a horizontal cask is about two meters, resulting in a lifted mass of 29 grams per cable. This results in a weight of 2.26 newtons per sensor. The system must also lift the sensor deployment mechanism, which must not rely on gravity for any of its actuation. Analysis of the data from the ultrasonic sensors also requires a sensor placement accuracy of one sensor diameter, which translates to 21.75 millimeters. The addition of some level of autonomy is also desired, especially because it could aid in guaranteeing that the cables do not tangle and the sensors are placed accurately.

1.4.6 Summary of Requirements

Demand/Wish	Requirement	Value	Unit
	Wall Adherence		
D	Robot Weight	Minimize	kg
D	Sensor Installation Force	Adhesive Dependent	N
D	Cable Weight	2.26	$N/cable$
D	Surface Roughness	Weld Steel[1]	
	Geometric		
D	Height	4	in
W	Height	2	in
D	Width	12	in
D	Length	20	in
D	Operable Cask Diameter	67.25	in
	Temperature		
W	Surface Temperature	410	K
D	Surface Temperature	330	K
W	Annulus Temperature	310	K
D	Annulus Temperature	300	K
	Radiation		
D	Gamma Radiation	2300	Roentgen/h
	Deployment Mechanism		
D	Carry Multiple Sensors	6	Sensors
W	Carry All Sensors	24	Sensors
W	Single User Input Deployment	Yes	
D	Easily Reloadable	Yes	
W	Quick Sensor Deployment	30	seconds
	Functional		
D	Prevents cable Entanglement	Yes	
D	Works in All Orientations	6	Orientations
D	Sensor Placement Accuracy	21.75	mm
W	Autonomy	Conditional	Level 3

Table 1.1: Specification of Requirements.

1.5 CaskClimber Prototype

The robot developed in this work, CaskClimber, includes two major elements that address the two primary objectives of the project, a suction based wall climbing robotic base to traverse the surface of the cask and carry a sensor to the desired location on its surface and a sensor deployment mechanism to permanently affix a sensor to the cask surface.

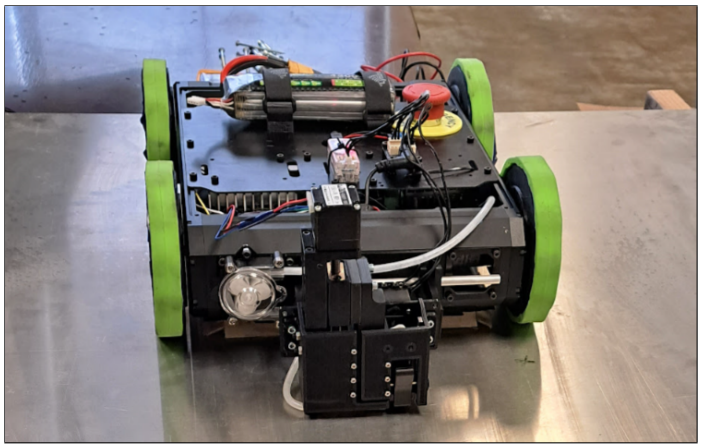

Figure 1.7: CaskClimber prototype.

For the robotic base an impeller-based suction system was developed, utilizing a commercially available brushless DC motor and controller in conjunction with a 3D printed impeller that was optimized using Computational Fluid Dynamics (CFD). To ensure functionality in all orientations, a flexible undertray skirt made from 3D printed Thermoplastic Polyurethane (TPU) was created, guaranteeing constant contact between the skirt and the curved surface of the cask.

[1]The surface roughness is highly variable from cask to cask, but for this effort we worked from the roughness of the cask sample provided to us by Orano.

The sensor deployment mechanism permits the storage and installation of up to six sensors sequentially. These sensors are each attached to a sensor carriage, enabling control over all six Degrees of Freedom (DOF) while the robot is positioned in any orientation and protecting the fragile solder joints on their surface. The process involves pushing the sensors down a storage magazine using a small lead screw and stepper motor, guiding them across rails towards a stamper, where they are securely positioned with the assistance of two small magnets. Subsequently, a liquid adhesive is dispensed by a peristaltic pump and the sensor is pressed down onto the surface of the cask. Both the final positioning and pressing steps are executed by a single servo motor, employing a mechanism inspired by the Geneva drive. This design approach minimizes the number of actuators required and ensures that the different parts of the mechanism do not interfere with each other or cause damage to the sensors.

1.6 Summary of Scope and Objectives

The work summarized here creates a prototype for adhering sensors to the surface of the stainless steel canisters within DSCs with accurate positioning and cabled connection to the outside of the cask. The objectives of the work are:

- Source or develop a wall adhering robotic platform.
  - Test the efficacy of the suction and drive systems on a range of surface curvatures.
- Develop a custom sensor package and deployment mechanism.

  - Integrate the deployment mechanism into the robotic platform.

- Demonstrate the prototype in a relevant testbed environment with active sensors.

Completing these discrete tasks enables future integration of the proposed sensor deployment mechanism into many different robotic platforms. It also demonstrates a pipeline for the deployment the Smart Structures Group's pioneering work onto DSCs. This aims to create the necessary conditions for the high level continuous monitoring of dangerous nuclear waste, leading to safer and more cost-effective production of nuclear energy.

The scope of the work presented in this report includes the development and integration of university prototypes for two major elements necessary to any proposed solution. It includes a detailed description and evaluation of the feasibility of each, as well as demonstrations of their capabilities. The scope of this work does not include design optimization, reliability analysis, or survivability analysis in the cask annulus environment. These steps would be necessary before a future iteration of this solution could be deployed to an active DSC. This work also did not achieve autonomy for the robotic system, this important feature is left to future work as well.

1.7 Organization

This thesis report has gone over the design requirements necessary for the operation of a robotic platform inside a DSC as well as for the sensor deployment mechanism. It compiles and comments on the many related solutions that have

been published in literature and that exist commercially. The literature review compares the capabilities of several different suction modalities and discuss literature and patents related to the deployment and installation of PZT sensors. It also introduces a simulation software package (SuctionSkirtSolver) that is designed to help study the failure modes of the wall climbing platform. The accompanying software should serve as a resource for future engineers approaching the problem of designing a suction and skirt based robotic platform for the inside of a DSC or any other non flat surface. It then introduces the CaskClimber prototype and summarizes the design choices made in the pursuit of a solution to this difficult problem. It first discusses the development of the robotic platform and the design considerations of the impeller, skirt, and drive subsystems. It then discusses the development of the sensor deployment mechanism, including the sensor carriage, sensor storage magazine, carriage actuation system, and adhesive applicator. It then presents real world testing of the robot platform and validation of the accuracy of SuctionSkirtSolver. It concludes with a discussion of the demonstrated capabilities of the CaskClimber prototype, its shortcomings, and a discussion of future work.

Chapter 2

Literature Review

In the first part of this chapter, we examine various wall climbing platforms documented in existing literature, highlighting their design principles and operational mechanisms to guide the design of the prototype presented in this thesis. Additionally, the chapter discusses and evaluates different methods employed in generating suction, a critical component for the secure adhesion and mobility of these platforms on vertical surfaces. Through this exploration, we aim to identify the strengths and limitations of each approach in order to select one to pursue.

In the second part, we provide a brief discussion of the effects that the DSC environment may have on any adhesive used to install PZT sensors for long-term monitoring. Then we discuss several dispenser mechanism patents to help guide the design of a sensor deployment mechanism necessary for the installation of PZT sensors.

2.1 Wall Climbing

There exist several paradigms for the adhesion of wall climbing robots. These include magnetic, pneumatic, and electroadhesion methods. Due to the high suction force requirements of the system and the nonmagnetic nature of the stainless-steel

cask surface, we have chosen to apply a pneumatic system for active adhesion. Within the area of pneumatic adhesion there are several strategies that have been applied, all of which are explored in the following literature review, including:

1. Propeller-Thrust
2. Rotational Flow Suction
3. Sliding Suction Cup
4. Suction Pump and Seal

2.1.1 Propeller-Thrust

Propeller-type wall climbing robots work by using propellers to generate thrust toward a surface. Their performance is mostly independent of the condition of the surface. Some propeller type robots are designed to fly as unmanned aerial vehicles as well as to adhere to surfaces. Drawbacks include high power consumption and low payload capacity. The field is very concentrated with many existing solutions, which are well described by the literature review by Mahmood et al. [13].

Alkalla et al. [14] is a representative example that applies well to our application. Their robot has been shown to operate effectively on curved surfaces that are not ferromagnetic (Figure 2.1b). With its lightweight design of 1.66 kilograms, the robot can only carry a payload up to 600g. Additionally, its propellers generate a maximum thrust force of 49N. Due to the lower payload capacity afforded by propeller-type designs, they are not ideal for our application, in which an entire ad-

ditional deployment mechanism must be added and six heavy coaxial cables must be lifted by the robot.

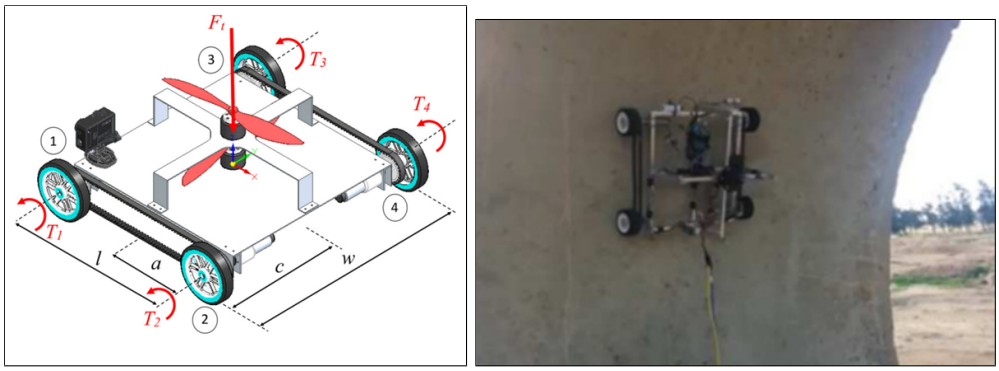

(a) Diagram. (b) Curved, nonmagnetic surface.

Figure 2.1: Alkalla et al. [14].

The propeller-type wall climbing modality offers low payload capacity, high power consumption, independence from surface condition, and independence from surface curvature. Our application requires adaptability to surface curvature and a tolerance for surface condition which are met by this modality. However, we require a high payload capacity from a small package, so the propeller-thrust modality falls short in that respect.

2.1.2 Rotational Flow Suction

Rotational flow suction systems generate a pressure differential by creating a vortex underneath the robot. This approach is promising as it does not require contact with the surface to maintain a pressure differential and is therefore adaptable to different surface conditions.

Zhao et al. [15] presents Vortexbot, which utilizes a vortex flow to generate suction force, as shown in Figure 2.2a. The authors provide a comprehensive evaluation of Vortexbot on walls with various surface conditions. Vortexbot is able to generate about 40 Newtons of force in the best case, with a performance decrease of about 28% at a roughness of 60 grit sandpaper and a performance decrease of about 38% with a clearance height of 10 millimeters. Patent US9738337B2 [16] describes this system.

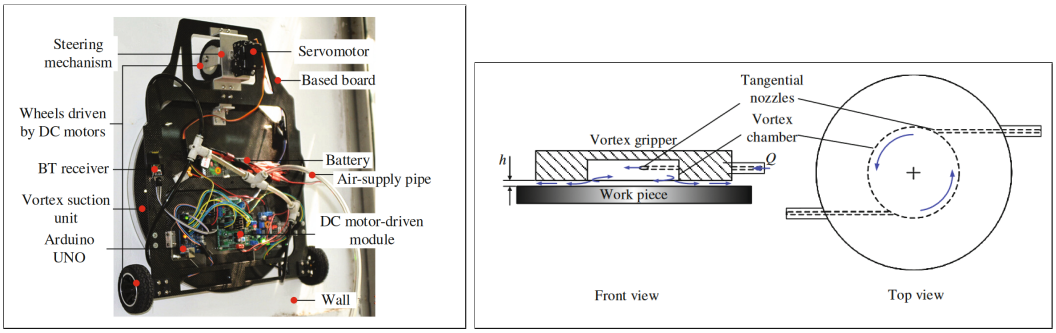

(a) Zhao et al. [15]. (b) US9738337B2 [16].

Figure 2.2: Rotational flow suction based designs.

Chen et al. [17] provides a comprehensive analysis of the design parameters that influence the effectiveness of the suction unit in a wall-climbing robot, shown in Figure 2.3a. An increase in clearance height (Figure 2.3c) is shown to have a large impact on the maximum suction force, which is a problem for use cases on curved surfaces where there are always regions with very large clearance heights regardless of the orientation of the robot. Experimental results revealed that, at best, their rotational flow design can create no more than 50 Newtons of suction force, which does not outperform the thrust based system.

(a) Photo.

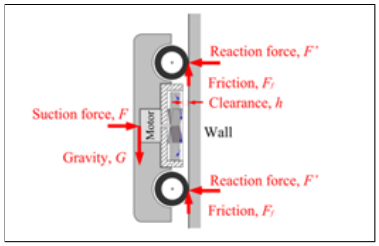

(b) Diagram.

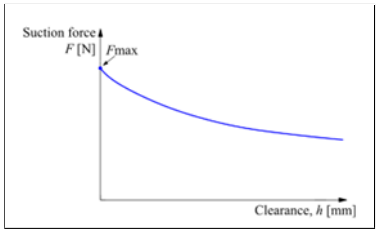

(c) Relationship between clearance height and potential suction force.

Figure 2.3: Chen et al. [17].

The rotational flow type wall climbing modality offers a low payload capacity, medium power consumption, low dependence on surface condition, and a high dependence on surface curvature. Because the rotational flow modality cannot tolerate very high clearances at the edges of its undertray, it is not ideal for very curved surfaces.

2.1.3 Sliding Suction Cup

The sliding suction cup modality utilizes a passive suction cup to generate the suction force needed for adhesion. It is an attractive option because it generates high suction forces with very low power consumption.

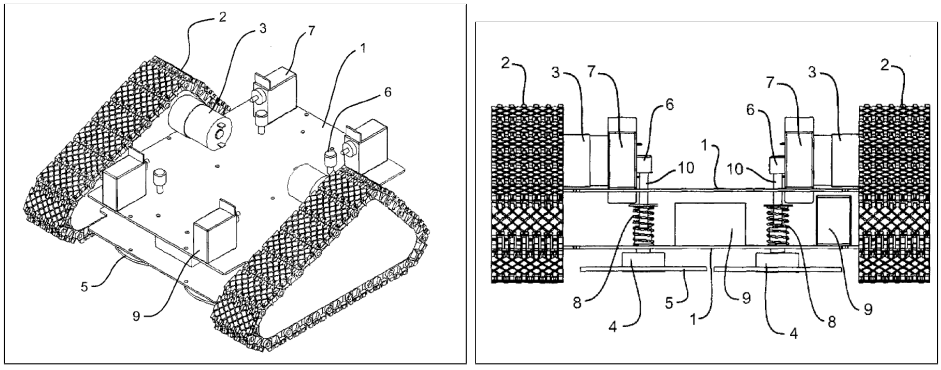

(a) Isometric view. (b) Front view.

Figure 2.4: Sliding suction cup based design [18].

Patent US9738335B2 [18] discusses a robot which utilizes a low-energy passive suction cup mechanism for adhesion, allowing it to move on inclined or inverted surfaces. The adhesion mechanism pushes down on a suction cup, creating a seal and a passive vacuum adhesion force. One major restriction of this design modality is that the passive suction cups require a very smooth surface quality to maintain suction and to slide. Unfortunately, the surface of the cask is not as smooth as the glass or food grade stainless steel surfaces for which this solution is designed.

The sliding suction cup type wall climbing modality offers a high payload capacity with low power consumption, but has a high dependence on surface condition. Sliding suction cup type wall climbers have not been demonstrated on surface roughnesses similar to our application. For this reason the sliding suction cup modality does not adequately meet our requirements.

2.1.4 Suction Pump and Seal

Many researchers have applied impeller based suction pump and seal systems in wall climbing robots. These work by applying a skirt sealing system and suction pump to create and maintain a negative pressure under the body of the robot. In this section we discuss several examples and pick out features of each that apply well to our application.

Yan et al. [19] presents a suction skirt robot shown in Figure 2.5 that is capable of performing remote-control inspections of nuclear storage tanks. The robot includes a driving mechanism, vacuum pump, discharge regulating valve, and a sealing skirt mechanism. The authors developed a closed loop control paradigm with the negative pressure sensor controlling the vacuum pump to ensure the robot could adapt to surfaces of different curvature, as shown in Figure 2.5. The authors describe its application for the inspection of DSC weld beads. This solution is designed to be teleoperated for expert visual inspection of the storage tank [19].

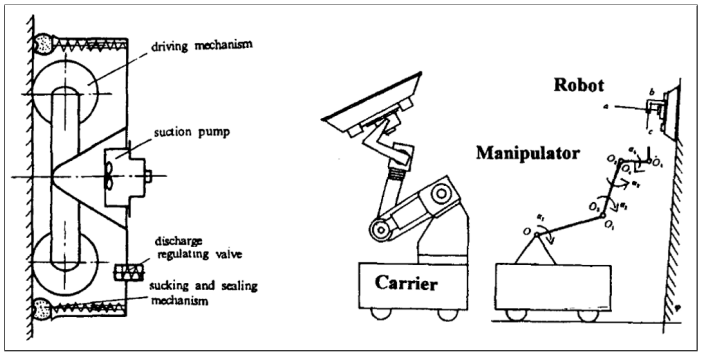

Figure 2.5: Yan et al. [19].

The robot described by this work almost exactly fulfills the requirements of

the work in this thesis, except for the addition of a mechanism for the permanent installation of sensors. This publication proves that an active suction based wheeled robot with flexible sealing skirt is capable of climbing the curved walls of nuclear storage casks, however, the exact details of their design are not shared in the publication and the performance of their system is not explored. The success of their study is promising.

Shujah et al. [20] presents a semi-independent wall climbing robot that operates wirelessly and is capable of climbing vertical surfaces and ceilings with a payload of 3 kilograms [20]. This payload capacity is very promising compared to the payload capacities reported for other suction modalities. Nishi et al. [21] present a similar design and provide an in depth analysis of the relationship between the suction pressure generated and frictional force available for wall climbing.

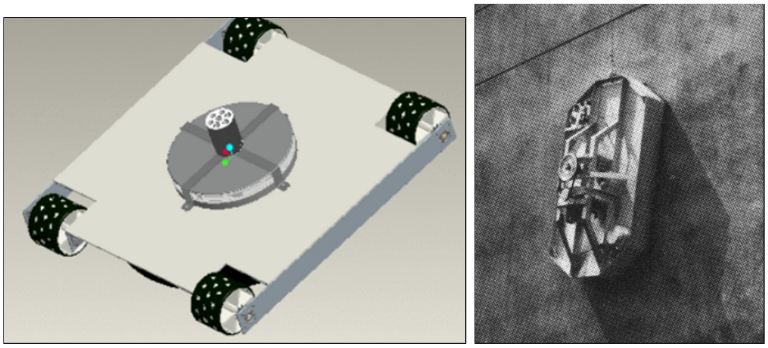

(a) Shujah et al. [20]. (b) Nishi et al. [21].

Koo et al. [22] present a wall-climbing robot system, referred to as 'LARVA', which was developed for visual inspection of structures with flat surfaces. The robot is equipped with two differential driving wheels with independent suspensions, shown

in Figure 2.7b. The adhesion mechanism is composed of an impeller and a double-layered suction seal, shown in Figure 2.7a.

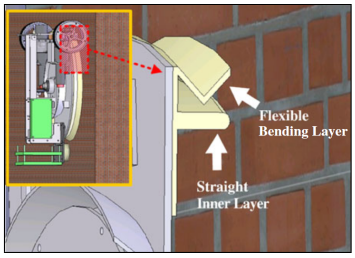

(a) Double layered sealing mechanism.

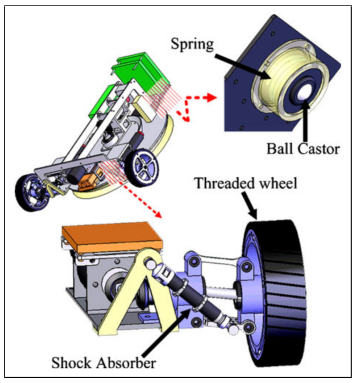

(b) Suspension and drive system.

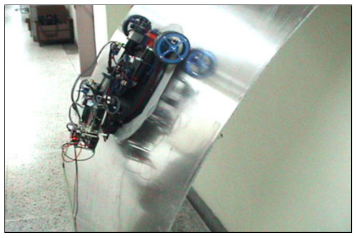

(c) Demonstration of curved surface adhesion.

Figure 2.7: LARVA; Koo et al. [22].

The authors provide static and aerodynamic modeling of the adhesion mechanism and carry out an analysis of adhesion, air leakage, and inner flow. The performance of the robot is experimentally verified for several surface conditions, including glass and concrete. The authors highlight that the robot was successfully attached to a curved surface, a very important requirement of the system being developed in this thesis. They demonstrated the ability to climb up the wall, change the direction of motion, and rotate. The authors call out several important challenges to the operation of a suction and seal based wall climbing robot. They stress the importance of a flexible sealing skirt and showcase their approach to the design of a double-layered sealing mechanism, and they highlight the tendency of the friction from the sealing skirt becoming too high and causing the drive wheels to slip. They attempted to

overcome this issue by adding a pressure sensor inside the sealing zone and a gyroscope on the body of the bot, creating a closed-loop control system for impeller. Li et al. [23] present a similar system, with the circular skirt and two drive wheel design. They demonstrate an ability to operate on rough surfaces such as a brick wall, but do not demonstrate any ability to operate on curved surfaces.

Fang et al. [24] presents a comprehensive study on the design and optimization of a wall-climbing robot's impeller. The study emphasizes the significance of the shape and sealing method of the negative pressure cavity on the adsorption performance of the wall climbing robot. The paper also highlights the importance of the impeller's structure in determining the size of the negative pressure. The main parameters of the impeller include impeller inlet diameter, blade inlet diameter, impeller outlet diameter, blade inlet size, blade outlet size, blade inlet geometric angle, and blade outlet geometric angle. They optimized these impeller parameters based on Computational Fluid Dynamics (CFD) model simulations and a genetic algorithm, increasing the performance of their impeller by 27.06%.

. These key impeller parameters and their effects were considered when we attempted to optimize an impeller for suction generation.

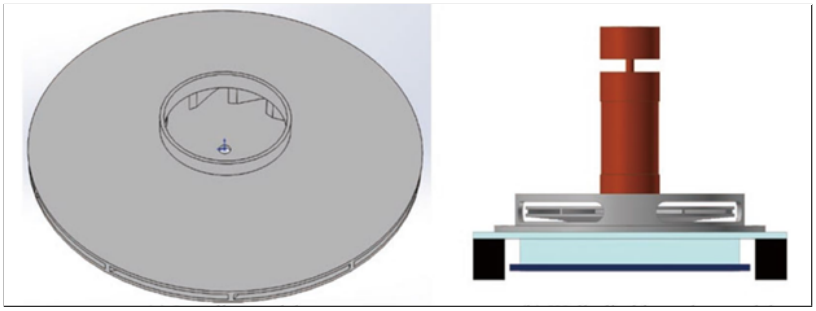

Figure 2.8: Fang et al. [24].

The study also explored the influence of robot orientation on the negative pressure value. The experimental results showed negligible differences in the negative pressure values of the wall-climbing robot in three different states: vertical, inclined 45°, and horizontal. It was concluded that the posture of the wall-climbing robot has no effect on the negative pressure value. This is an important result for the feasibility of the robot designed for this thesis.

The suction pump and seal wall climbing modality offers a high payload capacity and has been demonstrated on many surface conditions and on curved surfaces. These features meet all of the requirements of our application. The largest challenges are the surface condition of the canister, as DSC constructions are not uniform, and the curvature of the canister, as the skirt design is a recurring challenge in the literature. The system also has to overcome the friction generated by the skirt's contact with the surface, another challenge discussed in the literature.

2.1.5 Conclusions for Platform Design Review

Due to the limitation of the non-ferromagnetic surface material of DSC canisters, we elected to pursue a suction based option for adhering to the walls of the cask. Many suction based wall climbing robots have been developed and successfully deployed. Through this literature review we have identified the strengths of each, summarized in Table 2.1, to select the most effective option for our application.

Type	Payload Capacity	Power Consumption	Surface Roughness	Surface Curvature
Propeller-Thrust	Low	High	High	High
Rotational Flow Suction	Low	Med	High	Low
Sliding Suction Cup	High	Low	Low	Med
Suction Pump and Seal	High	Med	Med	Med

Table 2.1: Comparison of Wall Climbing Modalities.

Our application requires a high payload capacity to include a mechanism dedicated to the installation of sensors and to lift the heavy wires that are connected to them. It does not require a low power consumption as it can be tethered during operation, in fact a tether is necessary to manage the sensor wires and to facilitate retrieval in the event of a failure. The surface that it adheres to is smooth, but not as smooth as the glass and food safe stainless steel that the sliding suction cup modality requires. The surface is also significantly curved.

Motivated by the requirements (detailed in Table 1.1) and the capabilities of these four wall climbing modalities demonstrated in the literature and in industry (summarized in Table 2.1), we chose to pursue the suction pump and seal option.

2.2 Sensor Installation

Attaching PZT sensors to the surface of a DSC canister for long term monitoring requires both an understanding of the effects that environment may have on any adhesive used and a mechanical system to install those sensors autonomously. Here we provide a brief discussion of the use of adhesives with PZT sensors and explore several patents to help guide the design of a sensor deployment mechanisms.

2.2.1 Piezoelectric Sensor Installation

PZT sensors are a common tool used for structural health monitoring and have been studied extensively. Many works exist to explore the changes in performance of PZT sensors from changes in temperature and adhesive type. Although understanding the full performance profile of the PZT is not in the scope of this work, we discuss the effects of the adhesive used to attach it to the surface of the cask.

Qing et al. [25] explored the effects of adhesive thickness and modulus of elasticity and found that they both significantly effect the impedance, resonant frequency, and amplitude of the resultant signal. Sharma [26] compared the performance of cyanoacrylate and araldite adhesives at two temperatures, a reference temperature (15 °C) and elevated temperature (75 °C), concluding that cyanoacrylate worked better at an elevated temperature. Liu et al. [27] studied the effects of type of adhesive, adhesive thickness, accelerated aging, and elevated temperature on the performance of PZT sensors. They concluded that both shear strength and adhesive thickness have coupled effects on the performance of the sensors. Also, that during an elevated temperature test of 100 °C for 45 days performance increased after about 15 days

and then decreased again, concluding that the adhesive is unstable in the early stages of degradation but inevitably results in a decrease in performance. Shulz et al. [28] studied the effects of high temperatures on the performance of PZT sensors. They found that the performance degrades rapidly above 250 °F, restricting the application of the sensors to casks that are greater than five years old.

These works provide the essential background information needed to select the appropriate adhesive for attaching the PZT sensors to the surface of a DSC. This is crucial for long-term monitoring in an elevated temperature environment. We designed the adhesive applicator to use a liquid cyanoacrylate, but did not finalize an adhesive. To do so properly would require testing in a appropriate environment for an extended period of time and comparing the quality of signals that they can provide, and this was left to future work.

2.2.2 Dispenser Mechanisms

Few works were found describing dispenser mechanisms that could apply to the installation of small piezoelectric sensors. The search was restricted to mechanisms designed to dispense solid objects. Several relevant patents are discussed below.

Patent US2591855A [29] describes a stack of "thin flat articles", a spring to force them upwards toward the dispensing mechanism, and a slide to push each out in succession. It includes a latch to open and reload the mechanism from the spring side.

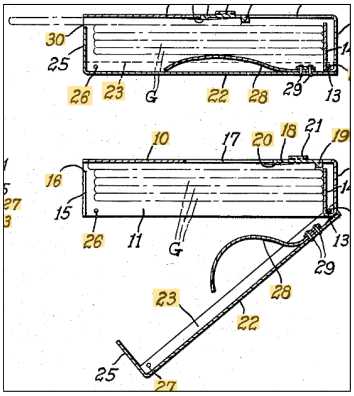

Figure 2.9: US2591855A [30].

Several more patents include similar sprung containers, but with slightly different methods of dispensing the object at the top of the stack. Patent US20070131705A1 [30] uses a motor that activates a wheel or belt. Patent US6425495B1 [31] uses a grasping mechanism that rotates to grab the object. Patent US3344951A [32] uses a spring loaded button to eject the object and reset the mechanism. Patent US5071033A [33] uses a hook attached to the underside of the cap to lift the object out of the stack. All of these approaches are shown in Figure 2.10.

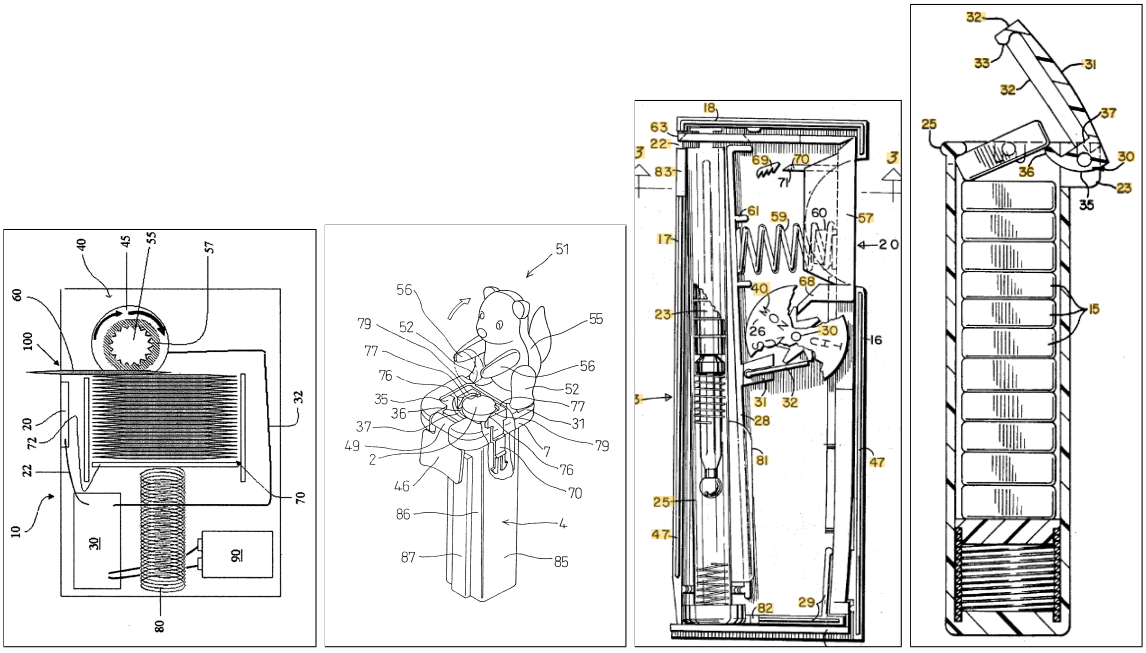

(a) US20070131705A1 [30] (b) US6425495B1 [31] (c) US3344951A [32] (d) US5071033A [33]

Figure 2.10: Patents with sprung containers.

Patent US5460295A [34] is unique from the rest because it couples the dispensing motion and container spring through a rotational element. This coupling of motions through a rotational element was an inspiration to our design as we attempted to decrease the number of actuations necessary for each dispensed item.

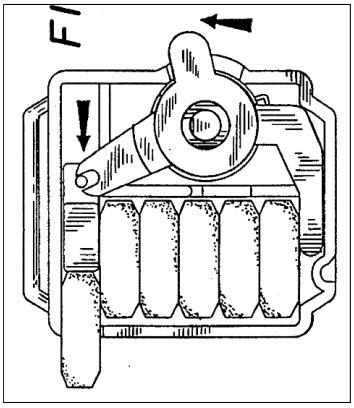

Figure 2.11: US5460295A [34].

The largest restrictions on our system are that it is required to work in all orientations and that is must work without any interaction from a human operator. This means that all of the patents discussed here fall short of fulfilling the requirements of our system, as they rely on either gravity or a human operator to aid in their behavior. Also, none of them include a mechanism for pressing the object onto a surface, another crucial requirement of our system.

For these reasons, a senior design team was commissioned to help generate new ideas [35][1]. Many of their key ideas were instrumental to the final design of the prototype presented in this thesis report, such as a stamper mechanism adjacent to the magazine with a slider to transition sensors from one to the other, a slot along the side of the mechanism to manage the sensor cables, and a pre-assembled sensor housing to protect the solder joints and control the sensor throughout the system.

[1]Contact the Nuclear and Applied Robotics Group directly for details and access to the senior design report.

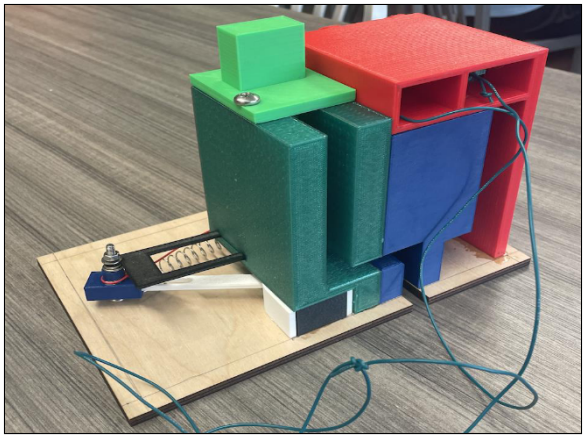

Figure 2.12: Project Resulting Prototype.

Chapter 3

Friction Balancing Tool: SuctionSkirtSolver

As discussed previously by Koo et al. [22] and others previously, balancing the friction resulting from the deflection of a flexible skirt and the friction from the drive wheels poses a significant challenge in a suction pump and seal based wall climbing platform. Consequently, we opted to develop a more mathematically rigorous approach for designing a suction robot suitable for cylindrical surfaces.

3.1 Overview of Approach

At its core, this approach utilizes a force balancing algorithm that takes multiple design parameters of the robot as inputs and produces a comprehensive report on potential failure modes. The static parameters considered include:

1. Robot mass and center of mass position.
2. Suction force, assuming consistent suction force as long as the skirt remains in full contact.
3. Dimensions, position, stiffness, and friction coefficient of the skirt.
4. Track, wheelbase, wheel radius, wheel stiffness, and wheel friction coefficient.

5. Cask radius.

The dynamic orientation parameters are spin and inversion. Spin is defined as the angle between the robot's heading and the major axis of the cask (X axis; Figure 3.1), while inversion refers to the angle between the robot's vertical axis and the direction of gravity. Two example orientations are shown in Figure 3.2 for clarity.

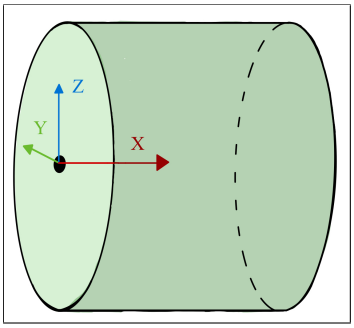

Figure 3.1: Demonstration of orientation definitions. Robot positioned on the z axis above the cylinder and facing the direction of the x axis is at zero spin and zero inversion. Spin is defined as a rotation about the z axis. Inversion is defined as a subsequent rotation about the x axis.

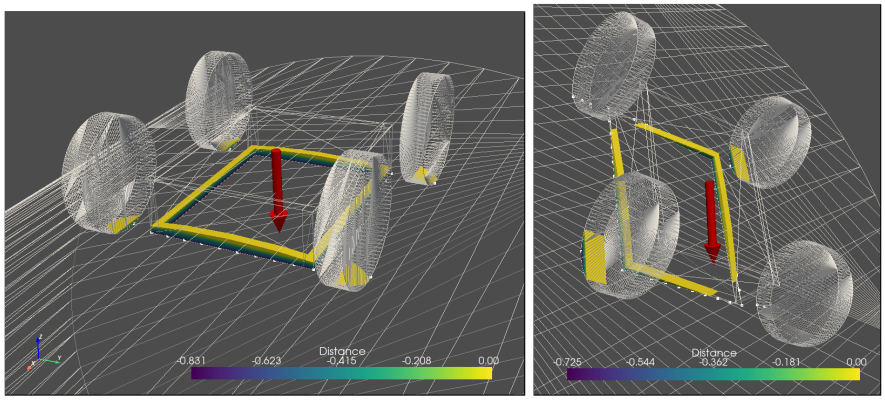

(a) Orientation 1 (b) Orientation 2

Figure 3.2: Example renders with spin and inversion set to (0,0) and (1,1). Overlap zones are shown and can be used to judge the performance of the robot qualitatively. In example orientation 2 it can be seen that the skirt loses contact in the corners and only two of the drive wheels have grip.

The analysis focuses on the two most critical failure modes identified during testing: loss of suction due to skirt contact failure with the cask surface (full contact condition), and the inability to move because of excessive friction from the skirt compared to the drive wheels (friction balance condition). Although it was not a common failure mode during the course of this research, the sliding condition (sliding balance condition) was also calculated as it was a problem experienced in the literature. The full contact condition is failed if any of the skirt is not intersecting the cask, as demonstrated in Figure 3.2b. The excessive friction condition is failed if the maximum static friction of the skirt is greater than the maximum static friction of the wheels. The sliding condition is failed if the component of gravity tangent to the cask is greater than the the maximum static friction of the wheels and skirt combined.

3.2 Force Balancing Calculations

A scalar optimization is conducted for each robot orientation using the Scientific Python Package (SciPy) [36] optimization tools to determine the radial robot position where forces achieve equilibrium [1]. The root finding method used was Brent's method with a bracketing interval, as this is the most efficient and reliable method offered in the SciPy package when the precise location of a sign change is known.

$$\sum F_{radial} = \vec{G} + \vec{S} + \vec{N}_{wheel} + \vec{N}_{skirt} \; as \; \sum F_{radial} \rightarrow 0 \tag{3.1}$$

The forces balanced include gravity, suction, and the normal force contributions of the skirt and wheels. In order to reduce the calculation to one dimension, the gravity is projected onto the normal direction between the robot and the surface. The suction force is assumed to be constant and in the same normal direction. It is important to note that the assumption of constant suction force is false when the full contact condition is failed, therefore other results are invalid in orientations where the full contact condition is failed. The normal forces created by the wheels and skirt are calculated based on the interference distance between the wheels, the skirt, and the cask surface. Friction conditions are derived from the normal forces and the static friction coefficients of the wheels and skirt.

The skirt and wheels are broken up into sets of points based on predefined resolutions. The normal force contribution from each is calculated from the depth of

[1] It is important to note that all other results are invalid in orientations where the force balancing optimization fails.

each point under the surface of the cylinder (Figure 3.3 and Equation 3.3) and their stiffnesses, as shown in Equation 3.2.

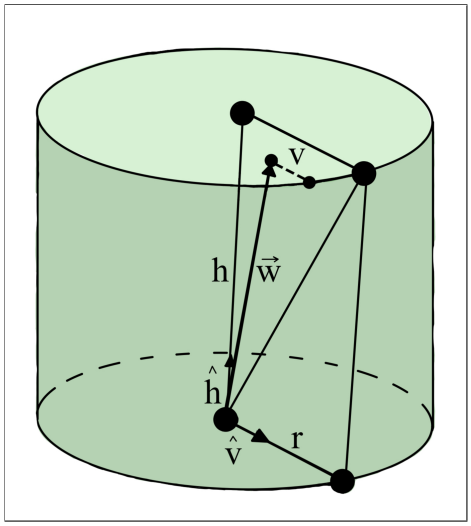

Figure 3.3: Diagram of intersection between given point and cask surface.

$$\vec{N}_{skirt} = \sum_{i=1}^{n} |\vec{v}_i| \times \mu \tag{3.2}$$

$$|\vec{v}_i| = \frac{-b + \sqrt{b^2 - 4ac}}{2a} \tag{3.3}$$

$$a = (\hat{v}_i \cdot \hat{v}) - (\hat{v} \cdot \hat{h})^2 \tag{3.3a}$$

$$b = 2[(\hat{v} \cdot \vec{w}_i) - (\hat{v} \cdot \hat{h})(\vec{w}_i \cdot \hat{h})] \tag{3.3b}$$

$$c = (\vec{w}_i \cdot \vec{w}_i) - (\vec{w}_i \cdot \hat{h})^2 - r^2 \tag{3.3c}$$

There the positive root of $\vec{v}_i$ is chosen as this is the intersection in the direction of positive $\hat{v}$.

3.3 Output and Analysis

To evaluate the CaskClimber prototype, the analysis was executed using empirical values from the robot. The coefficients of friction were approximately gauged by raising a stainless-steel sheet to the precise angle at which the components began to slip and then determining the coefficients from the tangent of the angle. The stiffness values were similarly approximated by computing the gradient of experimental displacement in relation to normal force values. A comprehensive list of these variables is presented in Table 3.1.

Variable Values Specific to this Robot			
Subsystem	Variable	Value	Unit
General	Mass	2.5	kg
	Suction	90	N
Skirt	Z-position	5	cm
	Width	18	cm
	Length	22	cm
	Stiffness	1	$\frac{N}{cm^2}$
	Friction Coefficient	0.31	N/A
Wheels	Track	26	cm
	Wheelbase	22	cm
	Radius	6	cm
	Stiffness	20.8	$\frac{N}{cm}$
	Friction Coefficient	0.58	N/A
Cask	Radius	122	cm
	Height	100	cm

Table 3.1: Variables used in the analysis of suction failure modes.

The results of this analysis are shown in Figure 3.4. In this example only the first 90 degrees of spin and 180 degrees of inversion were calculated. This is because

the robot being tested is symmetrical, and these limits can be changed for a non-symmetrical robot. Note that the results are null in the Friction and Sliding plots where the Full Contact condition is not met. This is because the constant suction force assumption is invalidated for those orientations.

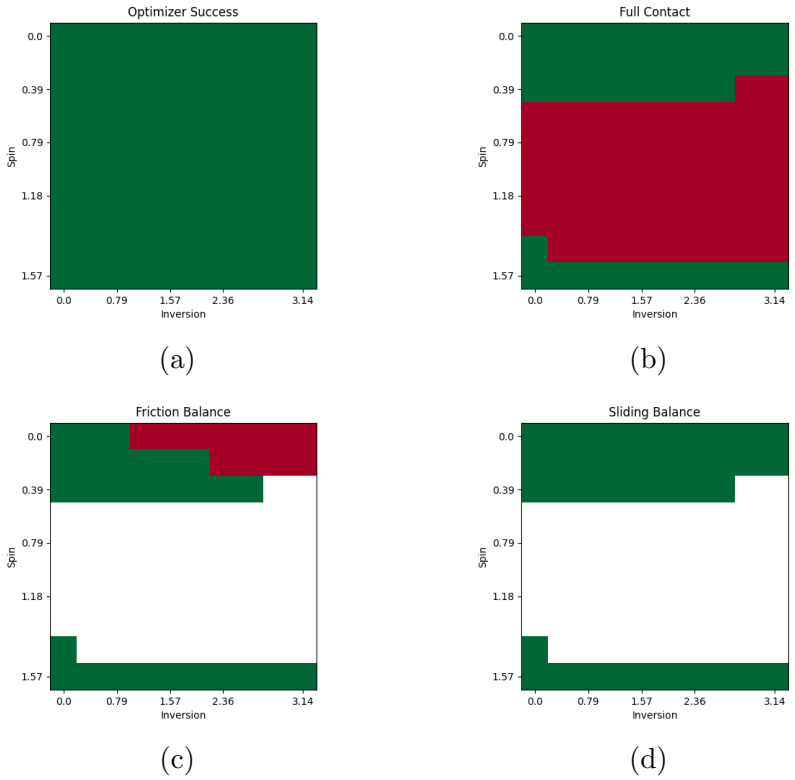

Figure 3.4: Results of simulation for real robot parameters at a cask radius of 85cm.

The most important result to highlight is the significant interdependence between the full contact failure and the spin variable, as seen in Figure 3.4b. Based on the results of this quantitative analysis and qualitative observations of the renders (the corners of the skirt out of contact as seen in Figure 3.2b), it can be concluded

that the largest contributor to the failure of the system is the rectangular shape of the skirt. The outcome may seem obvious, but it demonstrates the friction balancing tool's diagnostic capabilities. The accuracy of these results will be validated with real world testing of the CaskClimber prototype in Chapter 6.

This mathematical approach could be used to optimize robot parameters, treating the friction balance and sliding results as a cost function and the full contact results as a constraint. However, this optimization is left for future work as the parameter count is substantial, necessitating context-specific decisions about parameter ranges.

Chapter 4

Robotic Platform: CaskClimber

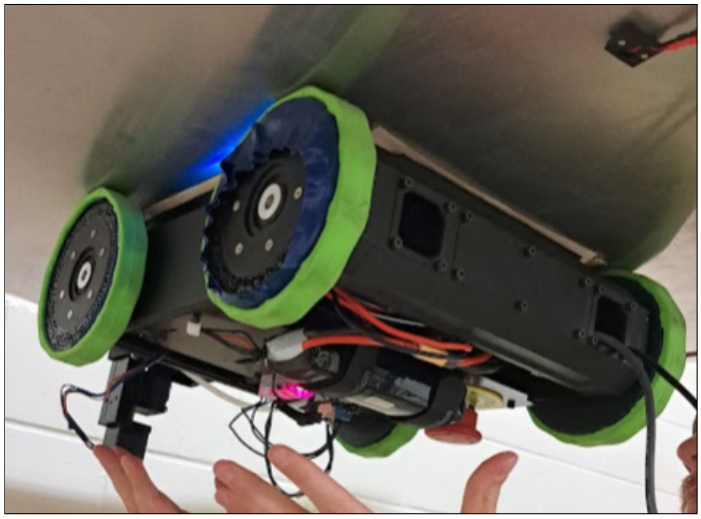

Figure 4.1: CaskClimber in operation fully inverted.

To access all areas of a DSC surface, a robotic wall-climber was developed: CaskClimber. Given the non-magnetic nature of the DSC's stainless-steel cask, an impeller-suction-based system was chosen. This method was favored because it generates a stronger suction force compared to other pneumatic adherence modalities.

The proposed concept entails having the robot placed onto the cask surface by a secondary robotic system, a component that has not been developed within the scope of this thesis. Subsequently, the robot navigates the cask surface, halting

intermittently to deploy sensors. The sensors are left behind with attached coaxial cables extending out of the overpack, from where the data can be collected and interpreted by the Smart Structures Group at any time.

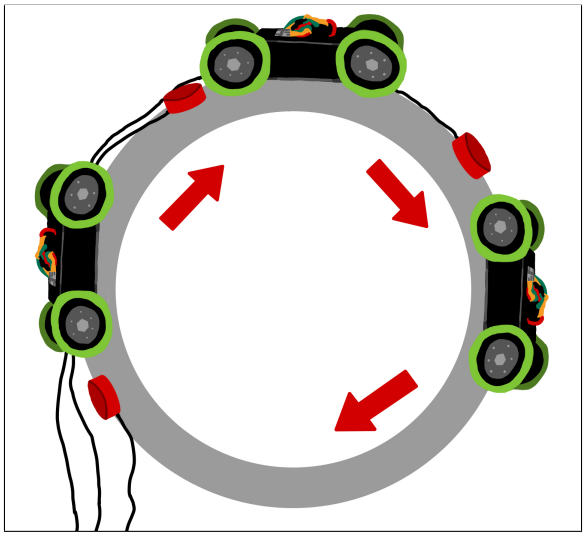

Figure 4.2: Motion Plan.

This chapter discusses the designs of CaskClimber's three major subsystems, the impeller, the flexible sealing skirt, and the drive system.

4.1 Impeller Design

The prototype integrates an impeller and a semi-sealed skirt, both of which have been designed to generate the necessary adhesion force for vertical surfaces. It utilizes a closed impeller, a design decision enabled by 3D printing. The design phase was an iterative process, including stages of 3D modeling, CFD simulation, and empirical testing for validation.

Upon achieving an effective impeller design, systematic testing was undertaken to find the optimal speed that would maximize efficiency. This experimentation was done by attaching the impellers to the end of a variable speed Dremel and an undertray with constant area. The assembly was then pulled with a spring scale until it lost contact and the weight of the assembly was subtracted from the readout to find the suction force. These examinations subsequently informed the selection of a Brushless DC (BLDC) motor with a KV rating of 2500, yielding an operational RPM of 30,000 with a power supply of 12 volts.

Following the determination of the ideal RPM, we leveraged CFD analysis using OpenFOAM [37] with the SimFlow GUI as shown in Figure 4.4b to identify and eradicate separation zones within the impeller. The design was further iterated upon, culminating in a significantly more efficient impeller. To augment the system's capabilities, a volute casing was introduced to the design as a diffuser, intended to decrease the velocity of the output while simultaneously increasing the pressure differential, as shown in Figure 4.3.

The finalized design successfully achieves a pressure differential of 0.35 pounds per square inch, which generates a suction force directly proportional to the undertray surface area. This results in a theoretical suction force of 31.5 pounds for the CaskClimber prototype. However, as the negative pressure within the skirt is not constant this can be taken as a maximum attainable value. It was experimentally found to be about 20 pounds.

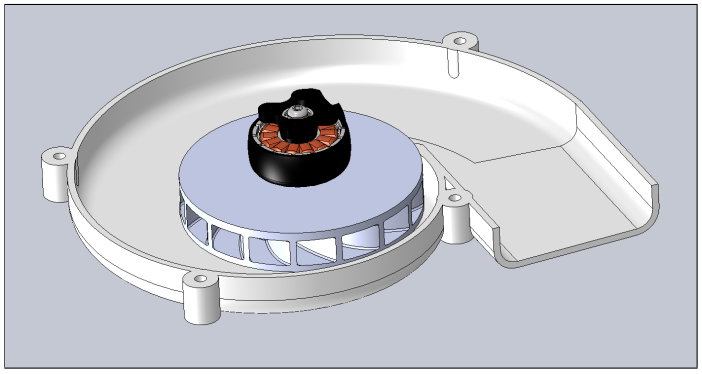

Figure 4.3: Impeller Assembly. The top half of the volute casing is removed so that the impeller and BLDC motor can be shown.

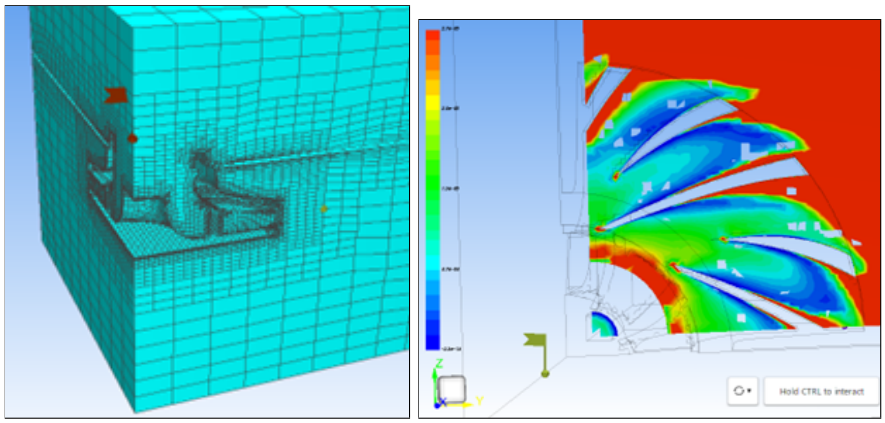

(a) (b)

Figure 4.4: Model used for CFD analysis and associated results. These are not of final results, but rather of a demonstration of the usage of CFD in the prototyping process.

4.2 Flexible Sealing Skirt

To ensure adaptability to the curved surface of the cask, a flexible undertray skirt was designed. It was designed to be fabricated with TPU using 3D printing,

allowing for quicker prototyping turnaround and flexibility [38]. The skirt's interior was lined with the loop side of a heat-resistant hook and loop fastener, functioning to establish a low-friction semi-seal. This design consideration aims to facilitate the robot's mobility while simultaneously enabling the generation of substantial suction forces. A heat-resistant material was used due to the high temperatures on the cask surface. The shape of the skirt's cross section also helps with maintaining contact with the surface, as it allows the negative pressure generated by the impeller to help force the skirt downwards, as shown in Figure 4.6.

The skirt was designed to be a rectangle to maximize the area and therefore the suction force generated by the system. With the width to length ratio of the CaskClimber, fitting the skirt into an inscribed circle would lead to a 30% decrease in surface area and therefore a 30% decrease in the maximum attainable suction force. However, the rectangular shape was found to have inadequate performance as the corners became failure points for the seal, especially when applied to a curved surface. In the future a circular skirt should be used, as was common in the literature. Avoiding catastrophic failure modes should be considered a higher priority than maximizing suction force.

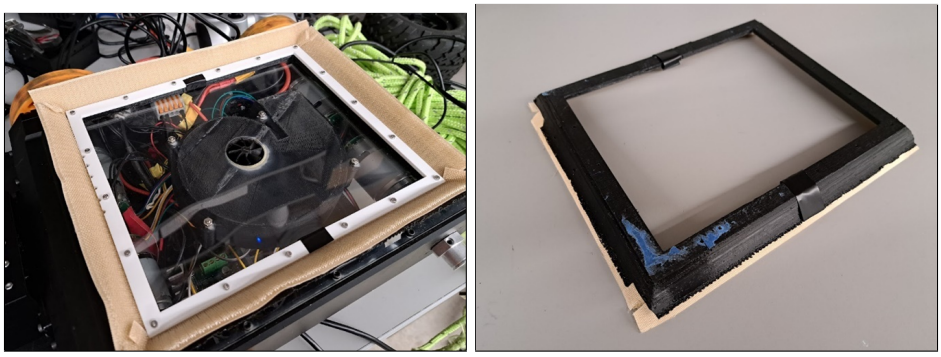

Figure 4.5: Flexible TPU skirt assembly.

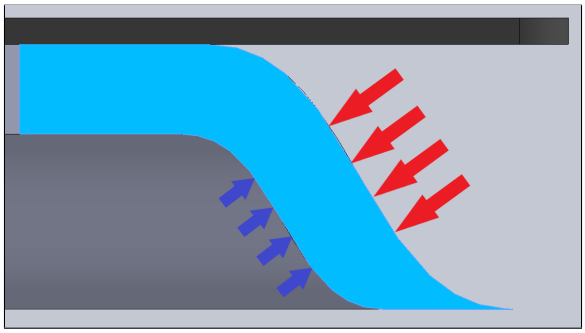

Figure 4.6: Skirt cross section to demonstrate the positive sealing effect of a pressure differential.

4.3 Drive System

The robot was designed with a direct drive system to avoid the extra weight and complexity of a suspension system. To handle the curved surface of the cask, the robot uses flexible wheels, which are meant to maintain effective traction at varying distances from the cask surface. They are constructed with three major layers: a plastic core to rigidly interface with the drive motors, a TPU tire to achieve a desirable stiffness, and a polyurethane rubber tread to generate a sufficiently high

friction coefficient between the wheel and the cask surface.

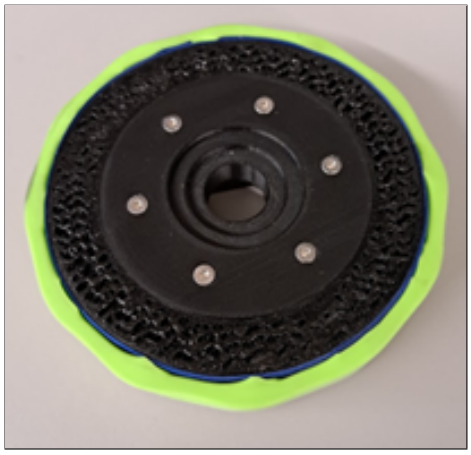

Figure 4.7: Wheel assembly.

The wheels used in the prototype were not flexible enough for the robot to operate effectively on the curved cask surface. The major failure mode was when the robot was oriented diagonal to the cask axis, in which case only two of the wheels were in contact. However, the wheels must be stiff enough in the other orientations to provide enough normal force to overcome the friction generated by the suction system and skirt. For these reasons, we believe that a suspension is necessary for a system to operate effectively on a curved surface, as was successfully demonstrated by Koo et al. [22]. Design of a suspension system is left for future work, but was not needed to validate the potential of this approach.

Chapter 5

Deployment Mechanism

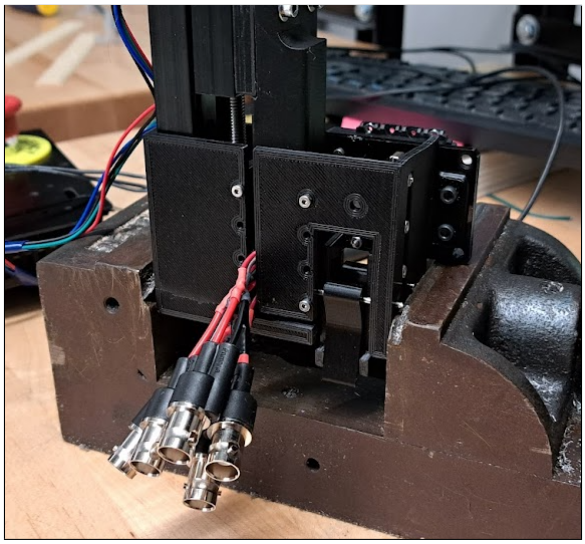

Figure 5.1: Sensor deployment mechanism assembly.

To meet the objective of permanently affixing sensors to the DSC surface, a specialized sensor carriage and deployment system was designed. This system preserves the delicate solder joints on the piezoelectric sensors, accommodates up to six sensors simultaneously, allows on-demand individual sensor installation, and functions across all orientations that the robot may encounter.[1]

[1]Video demonstration of the robot installing sensors in various orientations (https://youtu.be/tcZNsfQq5xU).

Achieving the objective of individually dispensing sensors from a stored stack necessitates four principal actuated motions: depressing the stack to expose each subsequent sensor (the magazine action), transitioning the sensor into a secondary column (the slider action), firmly positioning the sensor from the mechanism onto the cask surface (the stamp action), and dispensing adhesive to adhere the sensor to the surface (the adhesive application). These three movements are performed using three actively moving parts. To ensure that the slider and stamp actions do not obstruct one another, a novel mechanism inspired by the Geneva drive system was implemented to manage these operations.

In this chapter we discuss the design of the sensor carriage, the magazine action, the slider action, the stamp action, the Geneva inspired mechanism, and the adhesive application.

5.1 Sensor Carriage

A dedicated sensor carriage was designed to be permanently affixed to the piezoelectric sensor before installation. This carriage features a cavity to facilitate soldering leads to the sensor, along with a curved channel designed to redirect forces away from the solder joints and towards the carriage body, thus protecting the sensor's delicate solder joints (Figure 5.2).

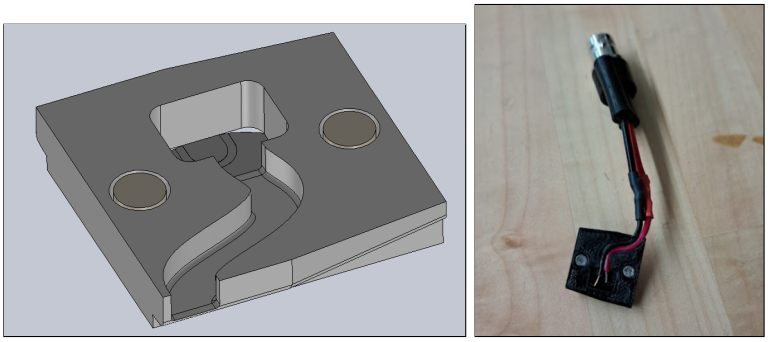

(a) CAD. (b) Fully assembled.

Figure 5.2: Sensor carriage design.

Additionally, the carriage incorporates two small magnets and multiple control surfaces to ensure correct alignment within the mechanism in any robot orientation. The carriage is also equipped with a Bayonet Neill-Concelman (BNC) connector to interface with the 20 AWG TE Piezoelectric Spiral Wrapped Coaxial Cables used by the smart structures team. This cable size is non-negotiable, given its importance in maintaining the necessary signal quality for the analysis carried out by the smart structures group.

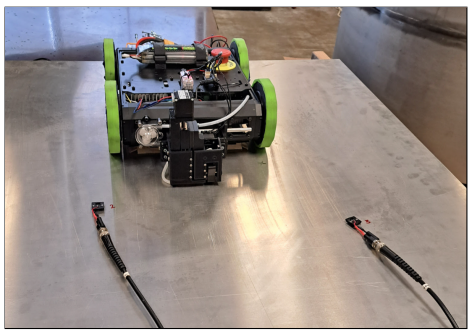

Figure 5.3: Demonstration of the sensor carriages being installed by the robot.[2]

5.2 Magazine Action

The magazine component was engineered to accommodate six sensors per reload, provide an easy refill process, and push sensors into the rest of the mechanism as each one is deployed.

The potential application of passive springs for the actuation of the magazine was examined as it was very common in the dispensation mechanisms explored in the patent search. However, this approach was deemed impractical, owing to the requirement for the mechanism to function in all orientations. Considering a maximum height of two meters, a cable weight of 14.5 g/m per cable, and a sensor carriage weight of 9.5 g, the spring would need to contend with a wide range of conditions. For instance, when the mechanism is inverted and the magazine is full, the spring must lift a total of 231g for the first sensor to be managed by the slider and stamp. Conversely, when the mechanism is upright with the spring in the same position, the slider must manipulate a sensor carriage that has 231g of weight with an additional 231g of spring force pressing down on it. As a result of these challenges, a COTS (Commercial off the shelf) lead screw and servo assembly were introduced to actuate the magazine. In the CaskClimbing prototype, this component exceeds the height requirement of the system. In future iterations it must be miniaturized or rearranged to fit.

[2]A test was carried out with the help of Nathan Wilson of the Smart Structures Group to confirm that the signal quality achieved was sufficient (https://youtu.be/u_q4JXicfg8).

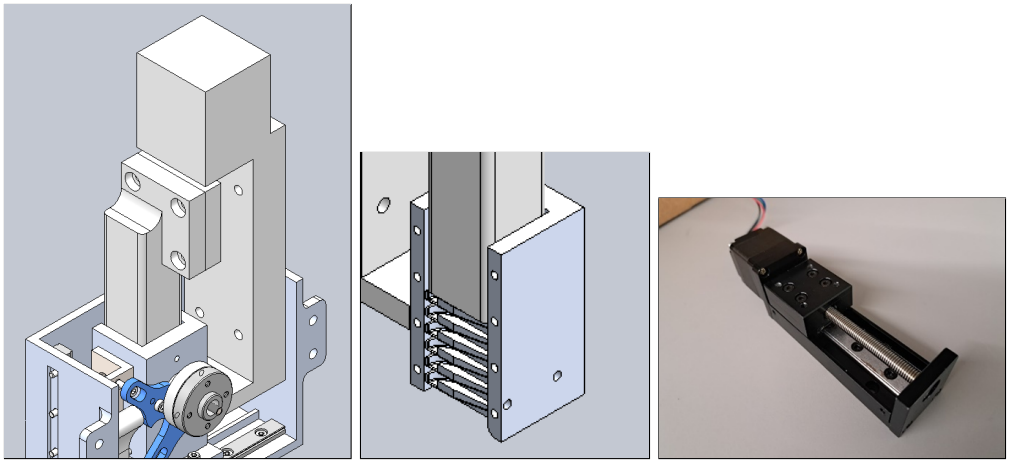

(a) Magazine assembly. (b) Sensor stack. (c) COTS lead screw.

Figure 5.4: Sensor magazine housing and lead screw assembly.

5.3 Slider Action

The slider mechanism incorporates two rails built into the chassis, along with a sliding component that moves along these rails. The sensor carriages are also designed to glide along these rails, facilitating their correct orientation as they're pushed down from the magazine and moved along by the slider. To reduce friction and ensure the slider's linear motion irrespective of the overall mechanism's orientation, the slider is also connected to a miniature linear ball slide. This structural setup ensures smooth, precise movement of the sensors through the deployment system.

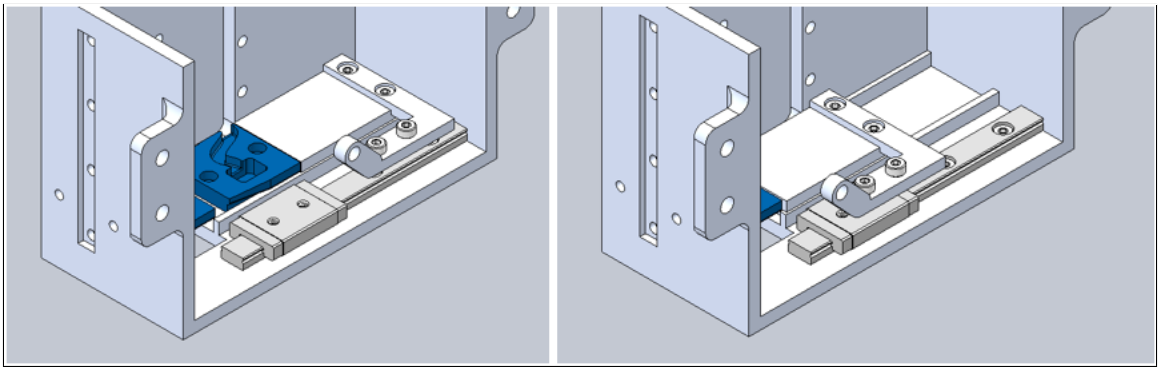

Figure 5.5: Slider mechanism stages of operation.

5.4 Stamp Action

Like the slider, the stamping mechanism is affixed to a miniature linear ball slide, which ensures its linear motion. The stamp's face is embedded with two small magnets that interact with the magnets in the sensor carriage, aiding in proper alignment. The stamp features two latches that secure the sensor carriage by its rail guides as it is inserted into the stamp. The operation of these latches is governed by static pins attached to the mechanism's chassis that mate with slots in the latch arms. This sliding contact compels them to open when the stamp is moved downward toward the cask's surface. As pressure is applied between the sensor and the surface, the latches completely open, ensuring a smooth and precise sensor placement in any orientation.

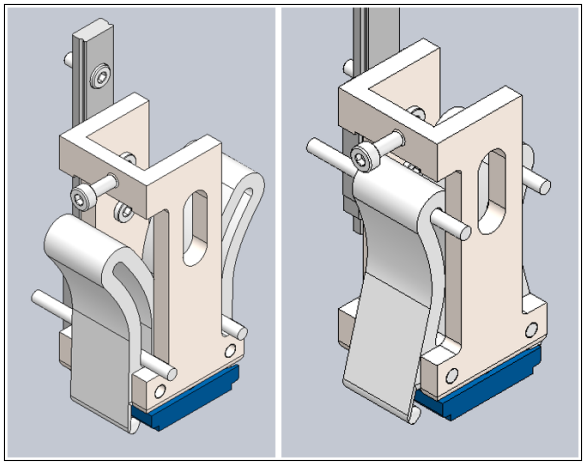

Figure 5.6: Stamp mechanism stages of operation.

5.5 Geneva Inspired Input

A mechanism inspired by the Geneva drive was utilized to actuate both the slider and stamp, ensuring they would never obstruct each other. A Geneva drive is a gear mechanism that converts continuous rotation into intermittent rotary motion [39]. This mechanism comprises two main parts. The driving wheel, the continuously rotating part, features an off-center mounted pin. The driven wheel, with slots typically four or six, cut into one side, moves intermittently.

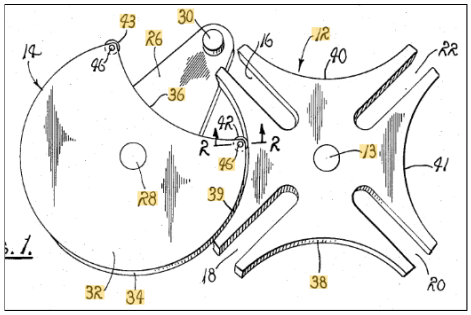

Figure 5.7: Geneva mechanism from Patent US3855873A [39].

In this application, the driving wheel is connected to a servo motor for precise control. The driven wheels are modified into arms that are connected to the linear rails of the slider and stamp subsystems. This arrangement allows a single rotational input to control two linear output motions without risk of interference.

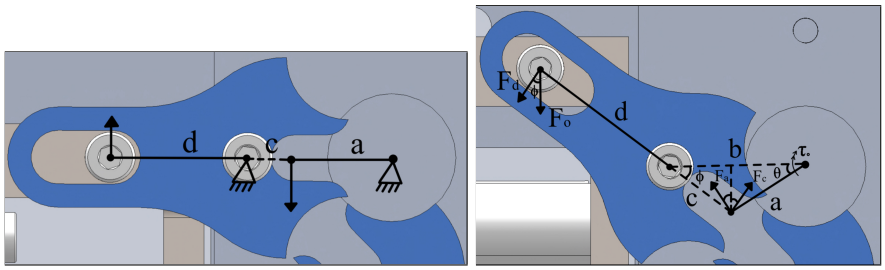

(a) (b)

Figure 5.8: Geneva mechanism force calculations diagram..

The primary drawback of the Geneva mechanism is the inverse force multiplication acting on the servo. The dimensions of the arms were chosen based on the linear range of motion required by each output and the space available for the driving wheel at the center. The range of motion of the output pin is governed by the equation:

$$\frac{2d}{\sqrt{2}} \tag{5.1}$$

Static moment calculations were conducted to determine the necessary servo strength and arm robustness for the system to function effectively throughout its range of motion. The forces required to manipulate the sensors are not very high, the maximum being the force required to lift the weight of one sensor and its trailing cable. This force is only 2.26N given a mass of 231g as discussed in Section 5.2. All

of the necessary equations were derived directly from the geometry of the system as shown in Figure 5.8. The inputs to the calculations are described in Table 5.1 below.

Geneva Mechanism Variable Values			
Variable	Slider	Stamp	Unit
a	7.63	7.63	mm
b	10.75	10.75	mm
d	12.5	10.25	mm
F0	2.26	2.26	N

Table 5.1: Geneva mechanism given variables for calculating required torque.

The full system of equations is shown in Equation 5.2 below. The system is simplified in Equations 5.3 and 5.4 for clarity.

$$c = \sqrt{a^2 + b^2 - 2ab\cos\theta} \tag{5.2a}$$

$$\frac{\sin\phi}{a} = \frac{\sin\theta}{c} \tag{5.2b}$$

$$\tau_0 = F_a a \tag{5.2c}$$

$$F_c = F_a \cos(\theta + \phi) \tag{5.2d}$$

$$F_d d = F_c c \tag{5.2e}$$

$$F_0 = F_d \cos\phi \tag{5.2f}$$

$$\phi = \arcsin\frac{a\sin\theta}{c} \tag{5.3}$$

$$\tau_0 = F_0 \frac{ad}{c\cos(\theta + \phi)} \tag{5.4}$$

The results of the analysis are shown in Figure 5.9, revealing that the maximum required input torque remains very low for the majority of the operative range, but spikes at 45 degrees. In practice the system often failed at that angle, and given that the Dynamixel A-12 servomotor that was used in this design has a stall torque of 1.5Nm, these failures start to make sense. This analysis should not deter future designers from employing the Geneva inspired mechanism proposed with this work, but rather lay the groundwork for proper motor sizing and geometric design considerations.

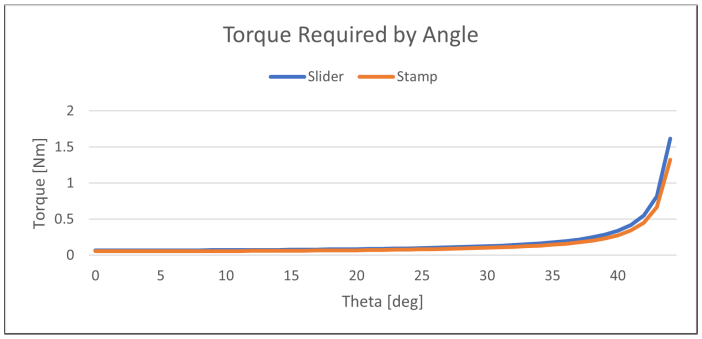

Figure 5.9: Geneva mechanism required torques across operation range.

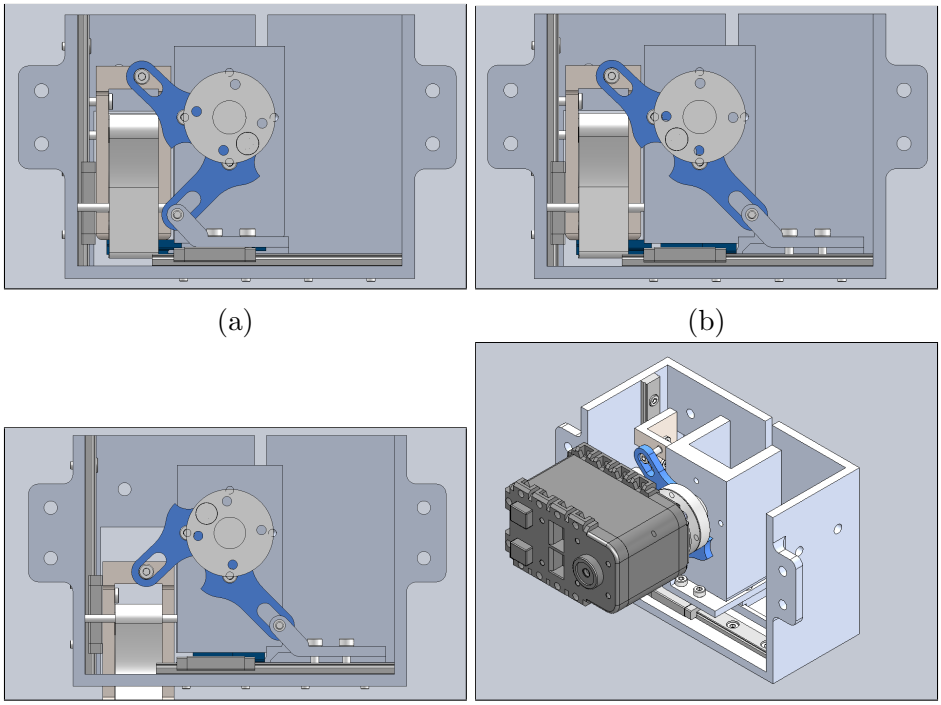

(a) (b) (c) (d)

Figure 5.10: Geneva mechanism stages of operation and isometric view.

5.6 Adhesive Application

The final crucial feature of this system is the adhesive dispensation between the sensor and the cask surface for permanent bonding. In this initial prototype, a peristaltic pump was employed to dispense controlled amounts of liquid adhesive onto the sensor during the stamping phase of deployment. The accuracy of dispensing small adhesive volumes via direct open loop PWM control was assessed, demonstrating considerable consistency and predictability, with a direct linear relationship between the PWM signal and the dispensed fluid quantity. The peristaltic pump was installed ad-

jacent to the deployment mechanism, with the tubing routed to the stamper system's exit.

The most significant limitation of this method is the potential for adhesive to drip into the deployment mechanism when it is in an inverted orientation, which could result in damage. The open end of the tube is also a large drawback as fast curing epoxies, like the cyanoacrylates used for testing, will cure in the end of the tube and cause failures. More work is needed to design a specialized adhesive applicator to overcome these challenges.

Several concepts were discussed to overcome these challenges, including the use of a spray nozzle to apply adhesive to the surface of the cask and preapplying adhesive to each sensor within a breakable seal to be released only when the sensor is pressed onto the cask surface. However, prototyping these ideas was not within the scope of this effort as the ideal adhesive for the heat resistance, radiation survivability, and signal quality requirements was not yet identified.

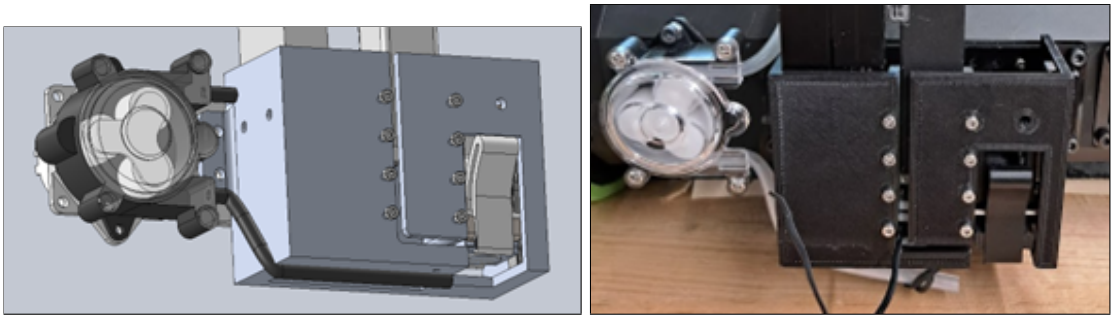

(a) CAD (b) Photo

Figure 5.11: Peristaltic pump attachment to the rest of the mechanism.

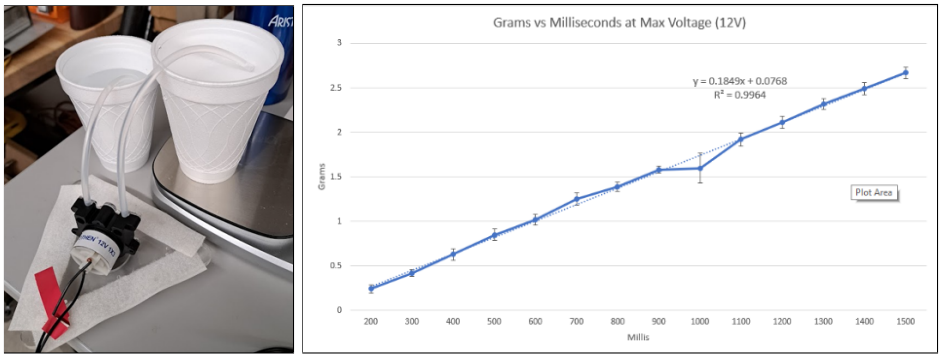

(a) Test Setup (b) Test Results

Figure 5.12: Peristaltic pump test to confirm repeatability of liquid dispensation.

Chapter 6

Testing and Validation

This section focuses on the real world testing that was carried out with the wall climbing robot platform. The failure modes being studied are the loss of suction pressure and the inability to drive due to excessive skirt friction. The sliding failure condition was not recorded as it was never encountered. The variable test conditions include:

1. Surface Curvature (as cylindrical radius)
2. Robot Spin
3. Robot Inversion

A testing jig was created to position a steel sheet to several equivalent radii for testing, it is shown in Figure 6.1. This jig worked by affixing two ratchet straps to the edges of a steel sheet and bending them to the correct "radius" by altering the length of the ratchet straps. Although the radius of curvature is not be constant with this method, the results are very similar due to the short length of the steel sheet with respect to the large radii being tested. The minimum radius tested was 85cm, the radius of a DSC canister, and the maximum radius tested was infinite (a

flat surface). Intermediate equivalent cylindrical radii that were tested were 108cm, 127cm and 190cm.

The jig was positioned at three levels of inversion as shown in Figure 6.1. The test procedure consisted of placing the robot at the center of the surface at full suction power, checking whether it could hold without falling, and then checking whether it could drive under its own power without becoming stuck. In this manner a 3x3 matrix of nine total data points was collected for each failure mode at each radius.

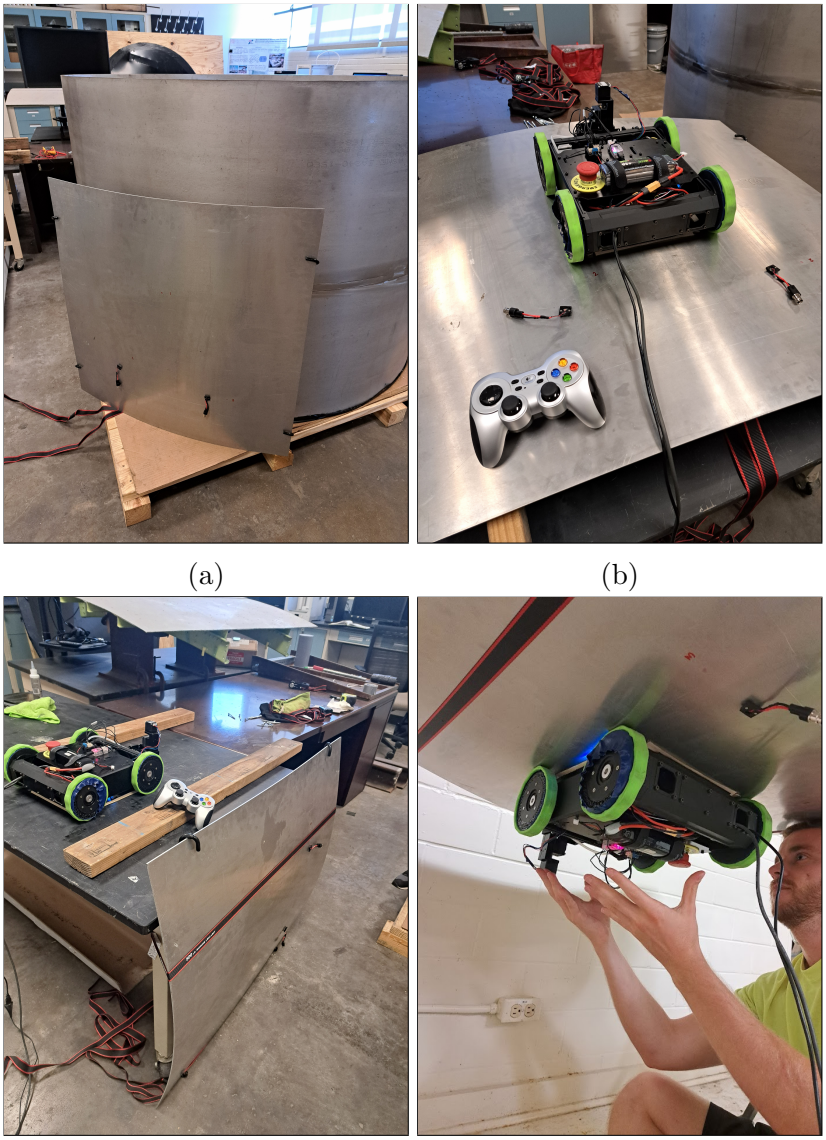

(a) (b)

(c) (d)

Figure 6.1: Photos of the performance testing setups. (a) The maximum curvature tested matched that of the real cask. (b) Testing performance at zero inversion. (c) Testing performance at 90 degrees of inversion. (d) Testing performance at full inversion.

The primary motivation for this testing with the real robot was to validate the accuracy of SuctionSkirtSolver, the friction balancing tool presented in Chapter 3. After running the solver for the same radii, Figure 6.2 shows that the optimizer found solutions for all orientations tested. Figure 6.3 shows the full contact and friction balance results side by side for the real world testing and friction balancing tool.

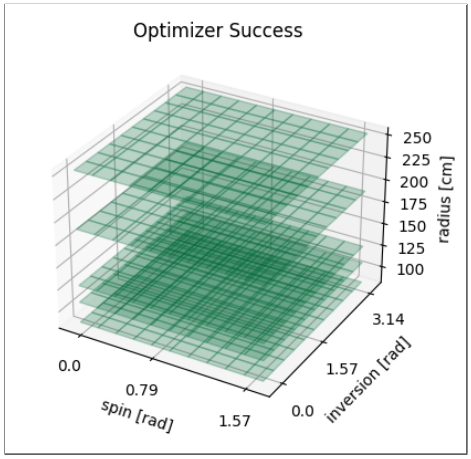

Figure 6.2: The success of the optimizer for all tested orientations to a tolerance of 1e-3 (1 mN).

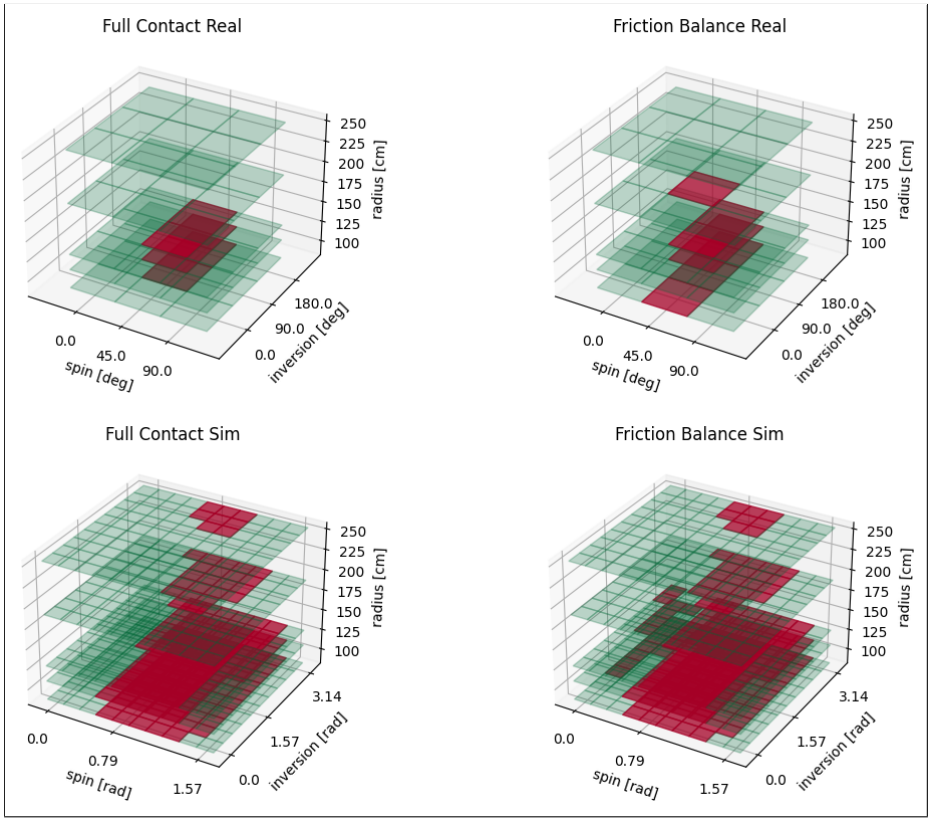

Figure 6.3: The failure modes studied for all tested orientations. The top row is data gathered through real world testing with the robot, and the bottom row is results of the simulator.

It is important to understand all of the shortcomings of the simulation results when compared to testing. The results of the simulation differ from the results of real world testing primarily due to the simplifying assumptions made. All stiffnesses were assumed to be linear, which is not true for either the wheels or the skirt. The coefficients of friction were empirically tested, and may not be sufficiently accurate or constant. The suction force was assumed constant, which is not true in practice but depends highly on the ride height of the skirt and the impeller power.

However, it is very encouraging to see general trends lining up well, such as the effect of spin on full contact and the effect of curvature on performance. This shows that the simulator could be a very useful tool in the early design stages. To show an example of using the simulator to explore the sensitivity of another variable, we will examine the effect of a change in skirt stiffness. It can be observed in this example (Figure 6.4) that a decrease in the stiffness of the skirt leads to an improvement in the loss of contact failure condition. Although this is not a full sensitivity analysis, it shows how the simulator can be used to explore the effects of different variables.

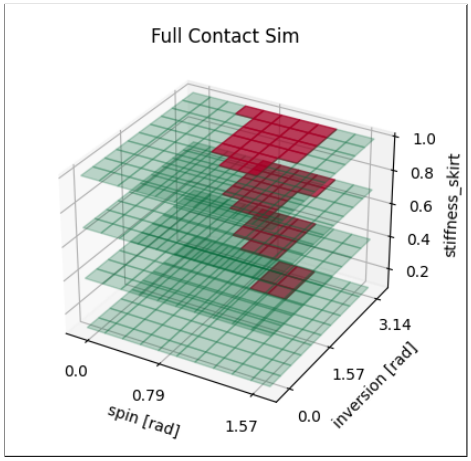

Figure 6.4: The full contact condition over a range of skirt stiffness values.

Chapter 7

Conclusions & Future Work

Nuclear power generation accounts for a sizable portion of electrical power production in the United States. Systems for managing the waste generated are a crucial part of the energy generation process. The current standard is DSC containers deployed near each power generation facility. As they age, they must be inspected to ensure that there is no damage to the integrity of the stainless steel cask within the large concrete overpack. These standard procedures entail removing the cask from the overpack to carry out an expert visual inspection. There have also been some demonstrations of a wall climbing robot being used to aid in inspection and preclude the need to remove the cask. Taking this one step further, the Smart Structures Group have pioneered a method to enable long term continuous monitoring of the condition of the cask using an array of PZT sensors permanently affixed to its surface.

This effort aimed to design and validate a wall climbing robotic system for the permanent installation of PZT sensors on the stainless steel walls of cylindrical DSCs. The specific requirements of a system deployed in the annulus of a DSC were discussed. A prototype robotic platform and sensor deployment system was proposed and tested to meet the requirements unique to the application relative to solutions found in literature. The results showed the design proposed is feasible, but does

not yet meet the reliability needed to be deployed inside a DSC. This will require additional engineering and testing as always for such nuclear environments.

Future work should include the addition of a suspension system for the drive wheels and a circular skirt. It could also include closed loop control of the suction pump impeller power based on a pressure sensor in the undertray or a gyroscope on the robot. This feature was explored in the literature but not applied to the prototype in this work. The addition of these features could have complicated the CaskClimber prototype, but were not necessary to evaluate feasibility.

The sensor deployment mechanism requires more professional manufacturing and an in depth exploration of its reliability. The issue of adhesive dripping must also be addressed in future designs.

SuctionSkirtSolver, a friction balancing calculator, was introduced with the purpose of finding viable design parameters for a suction-seal based wall climbing robot platform. The results of the calculator were validated by the results of testing with the CaskClimber prototype. It includes a visualizer to render the robot and explore its performance qualitatively. The calculator and visualizer will be made available for future researchers to accelerate the design process.

Future work could also include using the calculator to optimize the design parameters of a subsequent design iteration. The calculator could be embedded as the cost or constraint function in an optimization algorithm. This approach could lead to an optimal successive design proceeding this work.

The calculator could also be extended to include surface geometries beyond the

cylinder and skirt geometries beyond the rectangle. Also, the assumption of constant suction force should be replaced by a calculated value based on a controllable pressure differential and the encompassed skirt area. This would allow for the skirt geometry to be varied across iterations and the impeller power to be varied across orientations. It could also be extended to include a suspension system for the wheels, rendered as a spring in series with each wheel. These additions could improve its performance and usefulness. Finally, additional work is necessary to investigate the survivability of system components in radiation environments.

In conclusion, many of the design choices present in the CaskClimber prototype show promise and should be improved in future, such as the Geneva inspired sensor deployment mechanism and 3D printed TPU skirt, but many failed unequivocally and should be avoided in future, such as the direct drive and rectangular skirt. We hope that the findings presented in this thesis report help guide future researchers and designers.

Bibliography

[1] "Backgrounder on Radioactive Waste." [Online]. Available: https://www.nrc.gov/reading-rm/doc-collections/fact-sheets/radwaste.html

[2] E. Dehghan-Niri and S. Salamone, "A multi-helical ultrasonic imaging approach for the structural health monitoring of cylindrical structures," *Structural Health Monitoring*, vol. 14, no. 1, pp. 73–85, Jan. 2015, publisher: SAGE Publications. [Online]. Available: https://doi.org/10.1177/1475921714548937

[3] "Frequently Asked Questions (FAQs) - U.S. Energy Information Administration (EIA)." [Online]. Available: https://www.eia.gov/tools/faqs/faq.php

[4] U. S. G. A. Office., "Commercial spent nuclear fuel: Congressional action needed to break impasse and develop a permanent disposal solution," September 2021, gAO-21-603. [Online]. Available: https://www.gao.gov/products/gao-21-603

[5] "Dry Canister Storage System Inspection and Robotic Delivery System Development," EPRI, Palo Alto, CA, Tech. Rep. 3002008234, 2016. [Online]. Available: https://www.epri.com/research/products/000000003002008234

[6] D. G. Fobar, X. Xiao, M. Burger, S. Le Berre, A. T. Motta, and I. Jovanovic, "Robotic delivery of laser-induced breakdown spectroscopy for sensitive chlorine measurement in dry cask storage systems," *Progress in*

Nuclear Energy, vol. 109, pp. 188–194, Nov. 2018. [Online]. Available: https://www.sciencedirect.com/science/article/pii/S0149197018301811

[7] C. J. Lissenden, S. Choi, H. Cho, A. Motta, K. Hartig, X. Xiao, S. Le Berre, S. Brennan, K. Reichard, R. Leary, B. McNelly, and I. Jovanovic, "Robotic Inspection of Dry Storage Casks for Spent Nuclear Fuel," in *Volume 6B: Materials and Fabrication*. Vancouver, British Columbia, Canada: American Society of Mechanical Engineers, Jul. 2016, p. V06BT06A063. [Online]. Available: https://asmedigitalcollection.asme.org/PVP/proceedings/PVP2016/50435/Vancouver,%20British%20Columbia,%20Canada/285403

[8] ——, "Toward Robotic Inspection of Dry Storage Casks for Spent Nuclear Fuel," *Journal of Pressure Vessel Technology*, vol. 139, no. 3, Feb. 2017. [Online]. Available: https://doi.org/10.1115/1.4035788

[9] R. M. Meyer, J. Renshaw, K. Hunter, M. Orihuela, J. Stadler, K. Mauskar, U. Wolf, M. Klein, M. Weidmann, B. Bobbs, D. Dunn, and B. Lin, "Inservice Inspection of Extended Dry Storage of Spent Nuclear Fuel, Part II: NDE/Sensor Technology Development and Codification." American Society of Mechanical Engineers Digital Collection, Oct. 2021. [Online]. Available: https://dx.doi.org/10.1115/PVP2021-62069

[10] Y. Wu, J. Klein, H. Zhou, and L. Zuo, "Thermal and fluid analysis of dry cask storage containers over multiple years of service," *Annals of Nuclear Energy*, vol. 112, pp. 132–142, Feb. 2018. [Online]. Available: https://www.sciencedirect.com/science/article/pii/S0306454917303420

[11] P. L. Winston, "Inspection and Gamma-Ray Dose Rate Measurements of the Annulus of the VSC-17 Concrete Spent Nuclear Fuel Storage Cask," Tech. Rep. INL/EXT-07-13129, 926331, Sep. 2007. [Online]. Available: http://www.osti.gov/servlets/purl/926331-jv2dYJ/

[12] "Personal Annual Radiation Dose Calculator." [Online]. Available: https://www.nrc.gov/about-nrc/radiation/around-us/calculator.html

[13] S. K. Mahmood, S. H. Bakhy, and M. A. Tawfik, "Propeller-type Wall-Climbing Robots: A Review," *IOP Conference Series: Materials Science and Engineering*, vol. 1094, no. 1, p. 012106, Feb. 2021, publisher: IOP Publishing. [Online]. Available: https://dx.doi.org/10.1088/1757-899X/1094/1/012106

[14] M. G. Alkalla, M. A. Fanni, A. M. Mohamed, and S. Hashimoto, "Tele-operated propeller-type climbing robot for inspection of petrochemical vessels," *Industrial Robot: An International Journal*, vol. 44, no. 2, pp. 166–177, Jan. 2017, publisher: Emerald Publishing Limited. [Online]. Available: https://doi.org/10.1108/IR-07-2016-0182

[15] J. Zhao and X. Li, "Development of Wall-Climbing Robot Using Vortex Suction Unit and Its Evaluation on Walls with Various Surface Conditions," in *Intelligent Robotics and Applications*, ser. Lecture Notes in Computer Science, Y. Huang, H. Wu, H. Liu, and Z. Yin, Eds. Cham: Springer International Publishing, 2017, pp. 179–192.

[16] X. Li, "Climbing robot vehicle," U.S. Patent 9 738 337, Aug., 2017. [Online]. Available: https://www.freepatentsonline.com/9738337.html

[17] N. Chen, K. Shi, and X. Li, "Theoretical and Experimental Study and Design Method of Blade Height of a Rotational-Flow Suction Unit in a Wall-Climbing Robot," *Journal of Mechanisms and Robotics*, vol. 12, no. 4, Mar. 2020. [Online]. Available: https://doi.org/10.1115/1.4045652

[18] T. H. Davies, B. J. K. Sachdeva, L. G. Somerville, A. W. Taylor, J. G. Robertson, and X. Chen, "Robotic climbing platform," US Patent US9 738 335B2, Aug., 2017. [Online]. Available: https://patents.google.com/patent/US9738335B2/en

[19] W. Yan, L. Shuliang, X. Dianguo, Z. Yanzheng, S. Hao, and G. Xueshan, "Development and application of wall-climbing robots," in *Proceedings 1999 IEEE International Conference on Robotics and Automation (Cat. No.99CH36288C)*, vol. 2, May 1999, pp. 1207–1212 vol.2, iSSN: 1050-4729.

[20] A. Shujah, H. Habib, S. Shaikh, A. R. Ishfaq, H. Tahir, and J. Iqbal, "Design and Implementation of Semi-Autonomous Wall Climbing Robot Using Vacuum Suction Adhesion," in *2019 IEEE 17th World Symposium on Applied Machine Intelligence and Informatics (SAMI)*, Jan. 2019, pp. 275–280.

[21] A. Nishi, Y. Wakasugi, and K. Watanabe, "Design of a robot capable of moving on a vertical wall," *Advanced Robotics*, vol. 1, no. 1, pp. 33–45, Jan. 1986. [Online]. Available: http://www.tandfonline.com/doi/abs/10.1163/156855386X00300

[22] I. M. Koo, T. D. Trong, Y. H. Lee, H. Moon, J. Koo, S. K. Park, and H. R. Choi, "Development of Wall Climbing Robot System by Using

Impeller Type Adhesion Mechanism," *Journal of Intelligent & Robotic Systems*, vol. 72, no. 1, pp. 57–72, Oct. 2013. [Online]. Available: http://link.springer.com/10.1007/s10846-013-9820-z

[23] J. Li, X. Gao, N. Fan, K. Li, and Z. Jiang, "BIT Climber: A centrifugal impeller-based wall climbing robot," in *2009 International Conference on Mechatronics and Automation*, Aug. 2009, pp. 4605–4609, iSSN: 2152-744X.

[24] Y. Fang, S. Wang, D. Cui, Q. Bi, R. Jiang, and C. Yan, "Design and optimization of wall-climbing robot impeller by genetic algorithm based on computational fluid dynamics and kriging model," *Scientific Reports*, vol. 12, no. 1, p. 9571, Jun. 2022, number: 1 Publisher: Nature Publishing Group. [Online]. Available: https://www.nature.com/articles/s41598-022-13784-z

[25] X. P. Qing, H.-L. Chan, S. J. Beard, T. K. Ooi, and S. A. Marotta, "Effect of adhesive on the performance of piezoelectric elements used to monitor structural health," *International Journal of Adhesion and Adhesives*, vol. 26, no. 8, pp. 622–628, Dec. 2006. [Online]. Available: https://www.sciencedirect.com/science/article/pii/S0143749605001351

[26] S. Sharma, "Piezoelectric sensor voltage variation with different adhesives at elevated temperature," *IOP Conference Series: Materials Science and Engineering*, vol. 1225, no. 1, p. 012056, Feb. 2022, publisher: IOP Publishing. [Online]. Available: https://dx.doi.org/10.1088/1757-899X/1225/1/012056

[27] X. Liu, Y. Xu, X. Wang, Y. Ran, and W. Zhang, "Effect of Adhesive and Its Aging on the Performance of Piezoelectric Sensors in Structural Health

Monitoring Systems," *Metals*, vol. 10, no. 10, p. 1342, Oct. 2020, number: 10 Publisher: Multidisciplinary Digital Publishing Institute. [Online]. Available: https://www.mdpi.com/2075-4701/10/10/1342

[28] M. J. Schulz, M. J. Sundaresan, J. Mcmichael, D. Clayton, R. Sadler, and B. Nagel, "Piezoelectric Materials at Elevated Temperature," *Journal of Intelligent Material Systems and Structures*, vol. 14, no. 11, pp. 693–705, Nov. 2003, publisher: SAGE Publications Ltd STM. [Online]. Available: https://doi.org/10.1177/1045389X03038577

[29] J. E. Nicholson, "Chewing gum dispenser," US Patent US2 591 855A, Apr., 1952. [Online]. Available: https://patents.google.com/patent/US2591855A/en

[30] C. Behravesh and A. Behravesh, "Object dispenser," US Patent US20 070 131 705A1, Jun., 2007. [Online]. Available: https://patents.google.com/patent/US20070131705A1/en

[31] J. Senda and Y. Miyamoto, "Article dispensing apparatus," US Patent US6 425 495B1, Jul., 2002. [Online]. Available: https://patents.google.com/patent/US6425495B1/en

[32] N. A. Gervais, "Ejection pill dispenser with indicating means," US Patent US3 344 951A, Oct., 1967. [Online]. Available: https://patents.google.com/patent/US3344951A/en

[33] T. J. Siwek, "Tablet dispenser," US Patent US5 071 033A, Dec., 1991. [Online]. Available: https://patents.google.com/patent/US5071033A/en

[34] H. C. Law, "Candy dispensing system," US Patent US5 460 295A, Oct., 1995. [Online]. Available: https://patents.google.com/patent/US5460295A/en

[35] "Senior Design Projects." [Online]. Available: https://www.me.utexas.edu/academics/undergraduate-program/senior-design-projects

[36] E. Jones, T. Oliphant, P. Peterson *et al.*, "SciPy: Open source scientific tools for Python," 2001–. [Online]. Available: http://www.scipy.org/

[37] H. G. Weller, G. Tabor, H. Jasak, and C. Fureby, "A tensorial approach to computational continuum mechanics using object-oriented techniques," *Computers in Physics*, vol. 12, no. 6, pp. 620–631, Nov. 1998. [Online]. Available: https://pubs.aip.org/cip/article/12/6/620/510187/A-tensorial-approach-to-computational-continuum

[38] "Ultimate 3D Printing Materials Guide | Simplify3D." [Online]. Available: https://www.simplify3d.com/resources/materials-guide/

[39] R. Kenney, J. Fletcher, and R. Summers, "Geneva mechanism," US Patent US3 855 873A, Dec., 1974. [Online]. Available: https://patents.google.com/patent/US3855873A/en